Case Studies in Thermal Engineering 70 (2025) 106140

Contents lists available at ScienceDirect

Case Studies in Thermal Engineering

journal homepage: www.elsevier.com/locate/csite

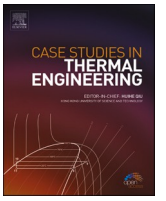

Accelerated discharging kinetics in zigzag- shaped triplex-tube latent heat storage with nano-modified phase change materials additives

Saleh Al Arni [a], Hakim S. Sultan Aljibori [b], Azher M. Abed [c], Hayder I. Mohammed [d], Jasim M. Mahdi [e], Hussein Togun [f], Abdellatif M. Sadeq [g,*], Mohammad Ghalambaz [h,**], Nidhal Ben Khedher [i]

[a] Department of Chemical Engineering, College of Engineering, University of Ha'il, P.Box 2440, Ha'il City, Saudi Arabia
[b] College of Engineering, University of Warith Al-Anbiyaa, Karbala, 56001, Iraq
[c] Air Conditioning and Refrigeration Techniques Engineering Department, Al-Mustaqbal University, Babylon, Iraq
[d] Department of Physics, College of Education, University of Garmian, Kurdistan, Kalar, 46021, Iraq
[e] Department of Energy Engineering, University of Baghdad, Baghdad, 10017, Iraq
[f] Department of Mechanical Engineering, College of Engineering, University of Baghdad, Baghdad, Iraq
[g] Mechanical and Industrial Engineering Department, College of Engineering, Qatar University, Doha, Qatar
[h] Department of Mathematical Sciences, Saveetha School of Engineering, SIMATS, Chennai, India
[i] Department of Mechanical Engineering, College of Engineering, University of Ha'il, P.Box 2440, Ha'il City, Saudi Arabia

ARTICLE INFO

Keywords:
Nanoparticles
Zigzag orientation
Energy discharge
Phase change materials

ABSTRACT

This study explores efficient schemes to substantially accelerate the discharge rates of phase change materials contained in a zigzag-shaped triplex-tube heat exchanger. It comprehensively investigates how zigzag geometry, heat transfer fluid flow parameters, and nanoparticle additives affect PCM discharge characteristics. Introducing a high 67.5° zigzag angle produced a 43.8 W solidification rate, which improves discharge rate by 10.6 % over straight tubes by increasing heat transfer area and promoting vortex formation. Extending the zigzag length to 15 mm further boosted the rate by 61.5 %–157.4 W by expanding the heat exchange surface area. Increasing the Reynolds number of the heat transfer fluid from 250 to 500 enhanced the solidification rate by 26 %–157.4 W by augmenting convective heat transfer. Lowering the heat transfer fluid inlet temperature from 20 °C to 10 °C dramatically reduced solidification time by 75 %, from 1956 s to 774 s by accelerating phase transition kinetics. Furthermore, adding 4 % aluminum oxide nanoparticles improved the rate by 16 %–182 W by enhancing thermal conductivity. Combining optimal parameters (67.5° zigzag angle, 15 mm length, 500 Reynolds number, 10 °C inlet temperature, and 4 % aluminum oxide nanoparticles) achieved a remarkable 300 % increase in discharge rate, from 39.6 W to 198.4 W compared to baseline straight tube configurations with pure phase change material.

* Corresponding author.
** Corresponding author.
E-mail addresses: as1004958@qu.edu.qa (A.M. Sadeq), m.ghalambaz@gmail.com (M. Ghalambaz).

https://doi.org/10.1016/j.csite.2025.106140
Received 12 December 2024; Received in revised form 10 March 2025; Accepted 13 April 2025
Available online 14 April 2025

Nomenclature

A_m	Parameter for velocity reduction in mushy zone, m^2/s	Greek symbols	
C_p	Specific heat capacity, kJ/kgK	β	Thermal expansion coefficient, 1/K
d_n	Nanoparticle diameter, m	λ	Liquid fraction
E_T	Rate of heat stored during solidifying mode	μ	Dynamic viscosity, Ns/m^2
E_e	Initial total energy of the PCM	ρ	Density, kg/m^3
E_i	Final total energy of the PCM	ϕ	Volume fraction of nanoparticles
g	Gravitational acceleration, m/s^2	∇	Gradient operator
h	Sensible Enthalpy, J/kg	Subscripts	
H	Total enthalpy, J/kg	e	initial
L	Latent enthalpy, J/kg	f	fluid
K	Thermal conductivity	HTF	heat transfer fluid
P	Pressure	i	final
S	Source term in the momentum equation	l	liquid
S_L	Source term in the energy equation	LHTES	Latent-heat thermal energy storage
t	time, s	np	nano-enhanced PCM
t_s	Solidifying time, s	PCM	Phase change material
T	Temperature	ref	reference
V	Velocity vector	s	solid

1. Introduction

Rising global energy consumption and mounting concerns over the depletion of fossil fuel resources and their environmental costs have made developing efficient and sustainable energy systems a crucial priority worldwide [1,2]. To mitigate the consequences of climate change and propose an environmentally friendly alternative to fossil fuels, renewable energy systems have been introduced and developed [3,4]. However, since renewable energy sources are weather-dependent, they need to be integrated with thermal energy storage (TES) components to compensate for the gap between energy demand and supply [5]. Among all TES mechanisms, the latent heat TES mechanism possesses the highest energy saving density; however, the discharging process of all TES mechanisms poses a challenge to a reliable TES system [6,7]. In fact, for a latent heat TES system, the discharging process is more important than the charging process, as the discharging rate is typically slow and ununiform [8,9]. Thus, it takes much more time to release the heat, which would cause a mismatch between energy demand and supply [10]. To address this problem, many approaches have been tried so far, including nanoparticle additives [11,12], fin insertion [13–15], reinforced PCMs [16], geometry alteration [17–21], metal foam insertion [22–25], and external effects i.e., magnetic field, rotation, tilt angle, and vibration [2,26,27].

As mentioned above, there are several techniques to make up for the shortcomings resulting from the weak thermal conductivity and low thermal diffusion rate of phase change materials (PCMs) employed in a latent heat TES system [28]. The use of high-conductivity materials (fins) has been suggested by many scholars, who advocate for their good performance toward better charging and discharging of PCMs. In a study conducted by Sun et al. [29], twisted fins were employed in a triplex-tube heat exchanger to examine the impact of fin configurations as well as its performance, and then the results were compared to the ones achieved for straight-fin and no-fin cases. They found that the use of twisted fins can reduce the discharging time by 22.9 % compared to the no-fin case. Also, they reported that twisted fins with the same volume fraction can enhance the solidification rate by 12.7 % in comparison to straight-fin cases. Nanoparticle additives are another approach that makes up for the low thermal conductivity of the PCMs. Mahdi et al. [30] carried out a study to examine the impact of alumina nanoparticle incorporation on the discharge behavior of PCM within a triplex tube heat exchanger. According to their results, dispersion of alumina nanoparticles with a volume fraction of 3–8 % can enhance the solidification time by 8–20 %. Scholars have reported the same achievements [31,32] through the use of other techniques that were mentioned above. However, some researchers [31,32] have shown that none of the aforementioned techniques alone is perfect, but that combining them can provide a viable solution. For instance, Khedher et al. [33] used fin-aided foam strip as a hybrid enhancer to address the limitations of erythritol as PCM. To further verify the enhancer's effectiveness, three other additives were introduced within the PCM container, including graphene nanoparticles, longitudinal fins, and foam strips. The findings revealed that the simultaneous use of foam, fin arrays, and fin-assisted foam strips resulted in a significant improvement in PCM solidification when compared to the sole use of nanoparticles. In a study conducted by Shahsavar et al. [34], wavy channels were taken into account for a vertically oriented double pipe heat exchanger. In their study, it was aimed to propose the optimum state of wave length by which melting, and solidification rates are enhanced. They reported that the use of wavy channels provided the latent heat storage system with the desired aggregation of the solid waves inside the heat storage medium realm. They also revealed that the optimum state of the wavy configuration could decrease melting and solidification times by 70.8 and 42.8 %, respectively, compared to the straight wall configuration. This shows the superiority of the geometry modification strategy toward better charging and discharging of the PCM without adding any additives to the system. In a similar study with similar boundary conditions, they [35] carried out an examination of the simultaneous effect of using porous medium along with wavy channel geometry and then compared their findings with those of straight walls and pure PCM. They concluded that the effect of wavy channels outstrips the use of porous medium since the amalgamation of wavy geometry with porous medium enhanced the melting and solidification rates by 91 and 94 %, respectively, and when compared to their results without porous medium [34], it is purely observed. Younis et al. [36] considered the corrugated plate heat exchanger in order to examine the heat storage and release rates. In their study, different wall configurations, including sinusoidal, square, triangular, and sawtooth wave profiles, were studied, and the results were compared to those of the flat wall heat exchanger.

They found that sinusoidal channels exhibited superior heat storage and release rates among all studied cases. There are also some other works [37] confirming the superiority of the geometry modification strategy toward enhancing the solidification rate of the PCMs.

Traditional cooling systems, such as cryothermostats, are energy-intensive, necessitating alternative solutions for efficient thermal management [38]. One promising approach is the integration of PCMs in systems requiring temperature regulation, such as solar panels, where different PCMs have been assessed for their cooling efficiency and impact on electrical performance [39]. Similarly, PCMs have been proposed as an alternative to conventional water-based cooling systems in Sono reactors, offering effective heat storage while minimizing energy consumption [40]. Beyond laboratory-scale applications, PCMs have also been explored for large-scale thermal management solutions, such as data centers, where LHTES components equipped with biomimetic fins significantly enhance heat recovery and reduce power consumption [41]. Bionic design strategies have further improved PCM performance by optimizing heat transport pathways, mimicking natural structures to enhance charge/discharge efficiency [42]. Tree-shaped fins have been shown to facilitate heat diffusion and accelerate phase change processes, highlighting the potential of innovative heat transfer structures in PCM-based thermal storage units [43]. The present study builds on these advancements by exploring novel PCM applications in thermal energy storage, providing insights into optimizing phase change processes for sustainable and efficient thermal management solutions.

Although the literature has fully considered different wall configurations to modify the PCM's characteristics, the zigzag pattern has not yet been examined. Talebizadehsardari et al. [44] modified the plate type of heat storage systems with a zigzag configuration for soldering PCM enhancement. The primary objective was to identify the optimal zigzag angle orientation for favorable outcomes. The study found that the optimum zigzag angle orientation was 60°, which results in a significant reduction of the solidification rate by 32.6 % compared to the case with a 30-degree angle orientation. In a research conducted by Wang et al. [45], a combination of geometry modification and multi-stage PCM was employed to increase the solidification rate. In their study, a zigzag pattern was used for the wall geometry, and the PCM container was divided into multiple stages designated for different types of PCMs. They reported that this combination imposes a good temperature shock, resulting in a faster solidification rate. Mahani et al. [46] similarly employed a zigzag pattern for a plate heat exchanger and reported a faster discharge rate compared to the flat wall configuration. The reason behind this is a greater heat-exchange surface, resulting in faster charge and discharge rates.

While previous studies have explored geometrical modifications like fins and pipes with longitudinal or helical patterns to enhance PCM discharge rates [19], the unique zigzag geometry has not been comprehensively investigated for triplex-tube containment systems. This study is the first to systematically analyze the effects of zigzag angle, zigzag length, HTF flow parameters like Reynolds number and inlet temperature, as well as nanoparticle dispersion on the solidification behavior of PCMs in a zigzag-shaped triplex tube heat exchanger. By identifying the optimal combination of these design factors, this work elucidates pathways to achieve remarkable improvements of up to 300 % in discharge rates over conventional straight tube systems. The quantitative insights into the fundamental heat transfer mechanisms and phase change kinetics governing PCM solidification in zigzag configurations are novel and address critical gaps in current knowledge. The findings can guide advanced thermal management strategies for diverse applications demanding efficient charging/discharging of PCMs like solar energy storage, waste heat recovery, indoor heating/cooling, and thermal regulation of electronics and energy systems. The study's unique approach bridges geometrical design, operational parameters, and nanocomposite materials to maximize solidification performance. This will provide valuable insights for PCM containment designs that lay the foundations for more efficient energy storage processes in LHTES systems.

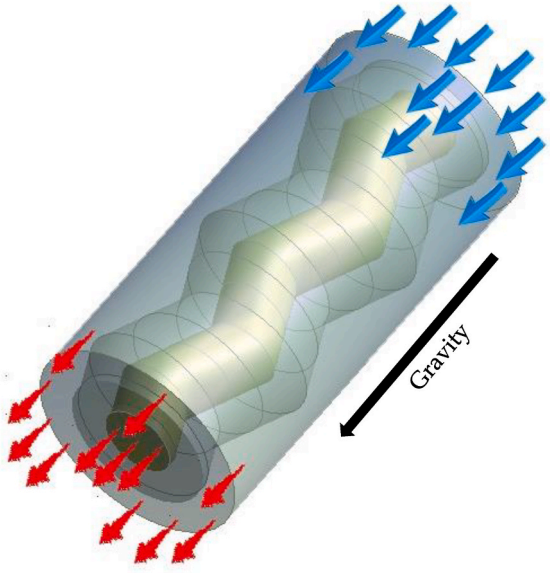

Fig. 1. Schematic of the zigzag-piped heat exchanger for the containment of PCMs.

2. Problem statement

This study is a numerical investigation without physical measurements. Fig. 1 illustrates the considered triplex-tube LHTES unit, which utilizes a NePCM in the central tube while H_2O serves as the heat transfer fluid (HTF) flowing through both the inner and outer tubes. Unlike traditional triplex-tube heat exchangers that employ straight tubes, the middle tube in this design features a zigzag pattern. To optimize the response rate of PCM during solidification, the interior and exterior pipes are configured to allow co-current flow of the operating liquid in the direction of gravity. This configuration has been demonstrated to exhibit superior performance compared to other fluid flow directions [47]. The HTF flows at an intake velocity of 2.69 mm/s in both the interior and exterior tubes, resulting in a Reynolds number of 1000. The total length of the tube is 250 mm, and the respective diameters of the inner, middle, and exterior pipes are 20, 40, and 60 mm, with a consistent length of 250 mm for all scenarios. The PCM container's capacity remains fixed throughout the whole investigation. Due to the inherent structural properties and the absence of rotational flow variations, the thermal characteristics of the system are analyzed under an axisymmetric condition.

The LHTES system under consideration, shown in Fig. 1, can be simplified to a two-dimensional axisymmetric model (Fig. 2) without compromising the accuracy of the results. This is justified by the fact that the triplex-tube geometry can be approximated as an axisymmetric system, as the heat transfer and fluid flow processes are primarily radial in nature, and the end effects at the inlet and outlet regions have a minimal impact on the overall performance [48]. Furthermore, the validity of the two-dimensional axisymmetric approach has been confirmed through the comparison of the numerical results with experimental data from the literature [49], as discussed in the following section. In this study, three zigzag tube angles corresponding to cases 1, 2, and 3 with angles of 27.5°, 45°, and 67.5° are examined (Fig. 2). Case 0 in Fig. 2 is the scenario with a straight center pipe. Case 3 with a 67.5° angle, corresponding to cases 3-H5, 3-H10, and 3-H15 in Fig. 2, is selected as the best instance for studying the impact of various zigzag lengths (5 mm, 10 mm, and 15 mm). The geometrical parameters are also shown in Fig. 2 for case 1.

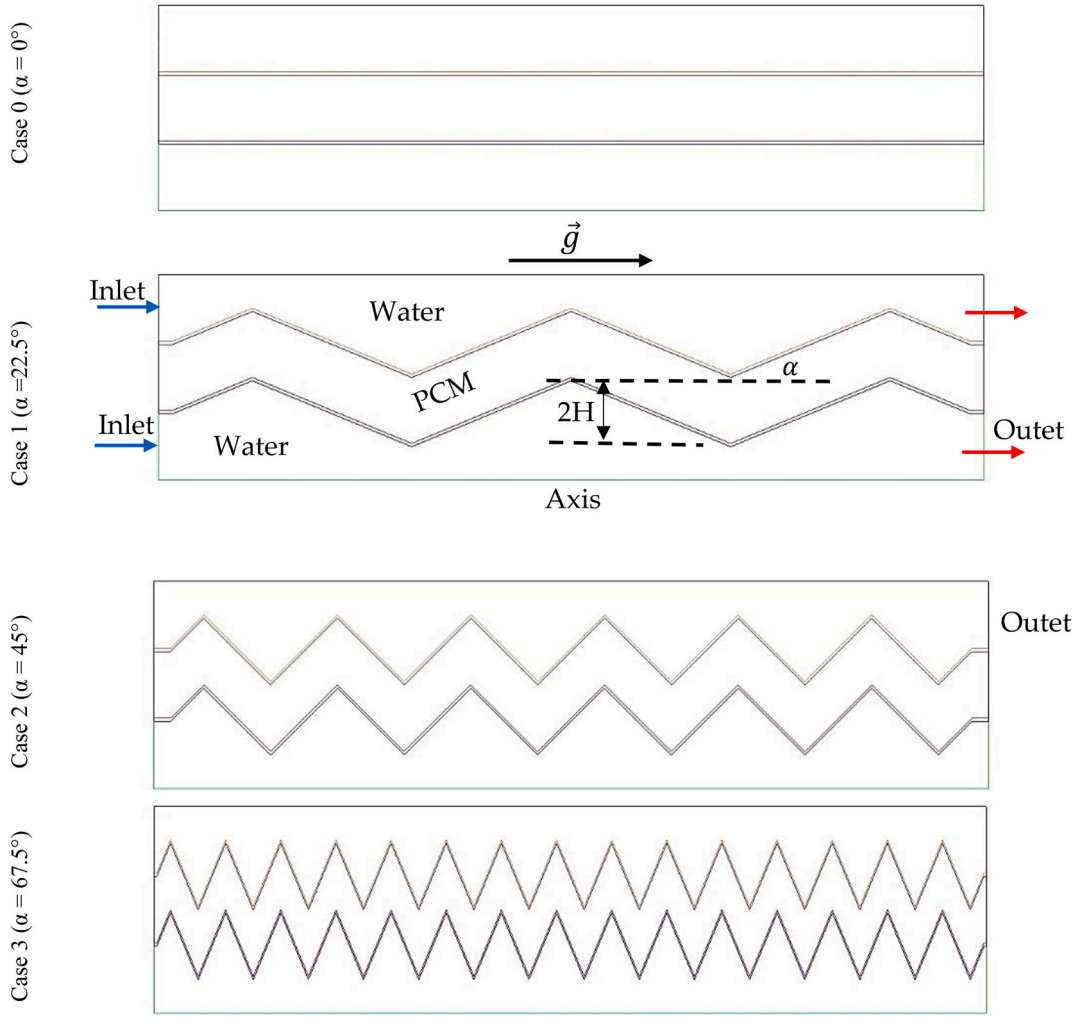

Fig. 2. The schematic of systems proposed in this study in 2D axisymmetric conditions.

The work focuses on exploring the impacts of introducing nanoparticles into PCMs, while also exploring the geometric characteristics of zigzag tubes. By analyzing different loading concentrations of 2 %, 4 %, and 6 % for various nanoparticles such as copper (Cu), copper oxide (CuO), alumina (Al_2O_3), and silver (Ag), the obtained outcomes are compared against the case where only PCM is utilized to quantify the improvements achieved through the introduction of nanoparticles. Paraffin RT-35 has been selected as the PCM of interest, primarily due to its solidification temperature being suitable for HVAC applications. The thermophysical properties of the PCM (RT35) and the nono-additive materials (Cu, CuO, Al_2O_3, Ag) were obtained from established literature sources, such as product data sheets [50] and previous studies [51,52]. Table 1 summarizes the thermophysical characteristics of RT-35, along with the characteristics of the nanoparticle materials under investigation.

The selection of nanoparticle concentrations (2 %, 4 %, and 6 % volume fraction) aligns with established findings in the literature that demonstrated effectiveness of these concentrations in enhancing performance without significantly increasing viscosity or agglomeration effects. Several studies ([19,53]) have shown that nanoparticle concentrations within this range provide an optimal balance between improved heat transfer and manageable flow resistance. Higher concentrations would tend to increase viscosity and reduce the overall efficiency of LHTES systems. The practical relevance of the present work is also demonstrated by the suitability of the LHTES unit's dimensions for use in confined building spaces, as depicted in Fig. 3. The figure illustrates the integration of the developed PCM-based LHTES unit within a building-integrated photovoltaic-thermal (PVT) collector. The thermal energy captured by the collector is transferred to the LHTES unit through a circulating HTF, enabling efficient storage of thermal energy. The stored thermal energy can be discharged to meet the building's thermal demand (e.g., space heating, hot water) when needed. Furthermore, the electricity generated by the PV cells can meet other electrical demands. So, the integrated system can effectively manage and distribute the generated electricity and captured thermal energy to meet the building's energy demands, leading to improved overall energy efficiency, reduced energy costs, and potentially lower carbon emissions.

3. Governing equations

The Enthalpy-Porosity technique is used for the numerical modeling of the proposed system. This technique assumes constant values of liquid fraction and porosity throughout the computational domain. Several key assumptions are made to establish the foundation for this study. The first assumption involves employing the Boussinesq approximation to enable the calculation of buoyant forces. Additionally, the flow of the liquid PCM is assumed to be transient, laminar, and incompressible. Moreover, the system is assumed to be oriented with gravity acting in the y-axis direction. Adequate insulation is implemented at the exterior boundaries to minimize heat transfer through those regions. Lastly, the solid edges of the system are assumed to experience no-slip boundary conditions. These assumptions collectively establish a framework for accurately modeling the system and analyzing the heat transfer behavior of the PCM within the triplex tube heat exchanger. The governing formulas are [19]:

$$\nabla.\rho_{np}\vec{V}=0 \tag{1}$$

$$\rho_{np}\frac{\partial\vec{V}}{\partial t}+\rho_{np}\left(\vec{V}.\nabla\right)\vec{V}=-\nabla P+\mu_{np}\left(\nabla^2\vec{V}\right)-\rho_{np}\beta_{np}\left(T-T_{ref}\right)\vec{g}-\vec{S} \tag{2}$$

$$\rho_{np}C_{p,np}\frac{\partial T}{\partial t}+\nabla\left(\rho_{np}C_{p,np}\vec{V}T\right)=\nabla\left(k_{np}\nabla T\right)-S_L \tag{3}$$

The momentum equation (Eq. (2)) is modified with a source term ($\vec{S}$) to account for the velocity reduction that occurs during PCM solidification [54]:

$$\vec{S}=A_m\frac{(1-\lambda)^2}{\lambda^3+0.001}\vec{V} \tag{4}$$

In the mushy zone where both solid and liquid phases coexist, the parameter A_m is used to idealize how fast the fluid velocity decreases as PCM solidifies. In this study, the value of A_m is chosen as 10^5 based on previous studies [19]. To evaluate the phase change progress, the liquid fraction of PCM (λ) is defined as:

Table 1
Thermophysical properties of the PCM and nono-additive materials [50–52].

Properties	RT35	Cu	CuO	Al_2O_3	Ag
ρ_l [kg/m^3]	770	–	–	–	–
ρ_s [kg/m^3]	860	8979	6000	3600	10500
Lf [kJ/kg]	170	–	–	–	–
C_p [kJ/kgK]	2	382	552	766	236
K [W/mK]	0.2	388	34	37	430
μ [N.s/m^2]	0.024	–	–	–	–
T_L [°C]	36	–	–	–	–
T_S [°C]	29	–	–	–	–
β [J/K]	0.0007	–	–	–	–

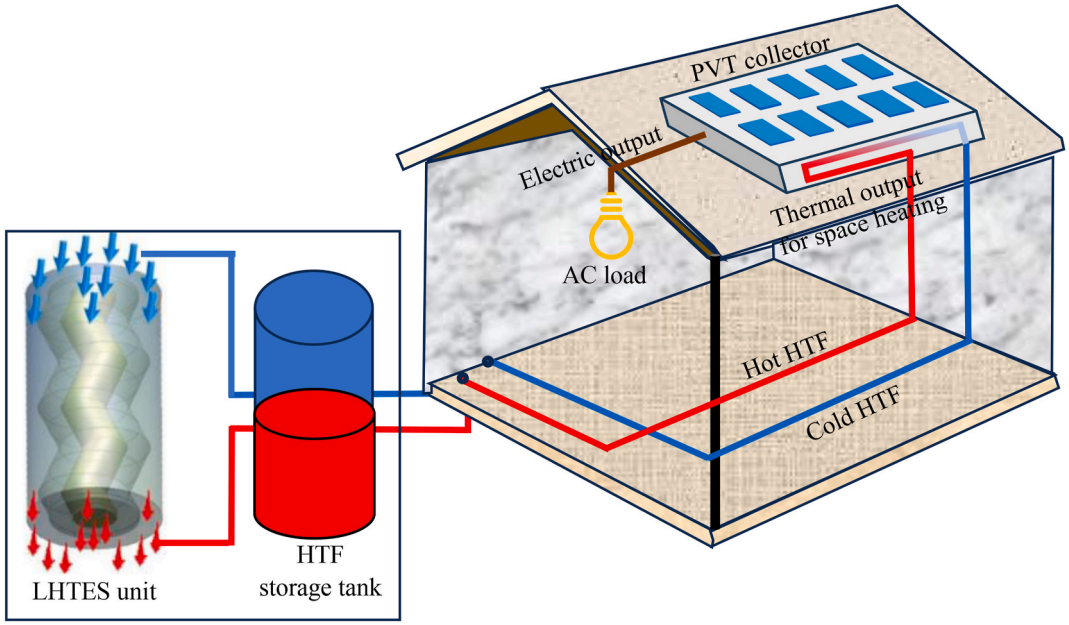

Fig. 3. Schematic view for the integration of the LHTES unit with building-integrated PVT collector for load shifting and energy management in buildings.

$$\lambda = \frac{\Delta H}{L_{np}} = \begin{Bmatrix} 0 \quad if \quad T < T_{Solidus} \\ 1 \quad if \quad T \rangle T_{Liquidus} \\ \dfrac{T - T_{Solidus}}{T_{Liquidus} - T_{Solidus}} \quad if \; T_{Solidus} < T < T_{Liquidus} \end{Bmatrix} \tag{5}$$

In this study, buoyancy-driven flow was modelled using the Boussinesq approximation, which assumed PCM density fluctuations are proportional to temperature variation. Buoyancy-induced convection currents vary direction and intensity with inner tube tilt, speeding up mixing and solidification. A less inclined or horizontal tube may stratify, when buoyancy forces are less and heat transmission is slower. Under the Boussinesq approximation, density is treated as a constant value in all governing equations, except for the buoyancy term in the momentum equation where it is calculated as [30]:

$$\rho_{np} = \rho_{np,ref}\left(1 - \beta_{np}\left(T - T_{ref}\right)\right) \tag{6}$$

In Eq. (3), S_L is calculated as:

$$S_L = \rho_{np} L_{np} \frac{\partial \lambda}{\partial t} + \rho_{np} L_{np} \nabla\left(\vec{V}\lambda\right) \tag{7}$$

The rate of heat stored during the soldifying mode ($\dot{E_T}$) is an another performance metric that is calculated as:

$$\dot{E_T} = \frac{E_e - E_i}{t_s} \tag{8}$$

where t_s is the soldifying time, E_e is the initial total energy of the PCM at the start of dicharging, and E_i is the final total energy of the PCM at the end of dicharging.

The introduction of nano additatives also affects other characteristics of base PCM, such as its density, specific heat, viscosity and latent heat. These thermophysical properties of NePCM depend on the volume fraction of nanoparticles in the nanofluid, which is the ratio of the volume of nanoparticles to the total volume of the nanofluid. The following equations show how the thermophysical properties of NePCM are estimated based on the volume fraction of nanoparticles and the properties of the base fluid and the nanoparticles [30]:

$$\rho_{np} = \phi\rho_n + (1 - \phi)\rho_{pcm} \tag{9}$$

$$C_{p,np} = \frac{\phi\left(\rho C_p\right)_n + (1 - \phi)\left(\rho C_p\right)_{pcm}}{\rho_{npcm}} \tag{10}$$

$$L_{np} = \frac{(1-\phi)(\rho L)_{pcm}}{\rho_{npcm}} \tag{11}$$

$$\mu_{np} = 0.983 e^{(12.959\phi)} \mu_{pcm} \tag{12}$$

$$\beta_{np} = \frac{\phi(\rho\beta)_n + (1-\phi)(\rho\beta)_{pcm}}{\rho_{np}} \tag{13}$$

$$k_{np} = k_{pcm} \times \frac{k_n + 2k_{pcm} - 2(k_{pcm} - k_n)\phi}{k_n + 2k_{pcm} + (k_{pcm} - k_n)\phi} + 5 \times 10^4 \beta_k L_f \phi \rho_{pcm} k_{pcm} C_{p,pcm} \sqrt{\frac{BT}{\rho_n d_n}} f(T,\phi) \tag{14}$$

where [30]:

$$f(T,\phi) = \left(2.82 \times 10^{-2}\phi + 3.9 \times 10^{-3}\right) / T_l - \left(3.067 \times 10^{-2}\phi + 3.91 \times 10^{-3}\right) \tag{15}$$

For the HTF section in the system, the governing equations (continuity, momentum, and energy) can be respectively expressed as the following:

$$\nabla \cdot V = 0 \tag{16}$$

$$\rho\left(\frac{\partial V}{\partial t} + V \cdot \nabla V\right) = -\nabla P + \mu \nabla^2 V + \rho\beta\left(T - T_{ref}\right)\vec{g} \tag{17}$$

$$\rho C_p\left(\frac{\partial T}{\partial t} + V \cdot \nabla T\right) = k\nabla^2 T \tag{18}$$

These equations describe the thermofluidic behavior of the heat transfer fluid under the influence of pressure forces, viscous forces, and gravitational forces, as well as the heat transfer due to conduction and convection effects.

4. Numerical solution and validation

The model of interest addresses the prediction of phase change in the proposed system using the standard SIMPLE algorithm to solve the pressure-velocity coupling throught the ANSYS Fluent solver. Momentum and energy calculations are performed using the QUICK scheme, while pressure correction is achieved through the utilization of the PRESTO method. To ensure convergence of the iterative solution, the termination criteria are set at 10^{-6}. In order to analyze the sensitivity of the mesh in use, different grid sizes (172016, 267002, and 419903 elements) and time steps (0.1, 0.2, and 0.4 s) are compared. Table 2 displays the discharging period corresponding to each mesh element count. The results indicate almost similar outcomes for 267002 and 419903 mesh elements, leading to the selection of 267002 as the appropriate number providing the best computational const for this research. The impact of time steps on the solidifying time is also examined, demonstrating consistent findings across various time step sizes. Ultimately, a time step of 0.2 s is chosen for the purpose of this research.

The numerical model developed in this study was validated by comparing its simulation predictions to experimental measurements from Al-Abidi et al. [49]. Their work examined PCM solidification in a triplex-pipe containment with longitudinal fins. Fifteen thermocouples placed at various radial and angular locations measured the PCM temperature distribution. Reference points matching these thermocouple locations were defined in the present simulations for validation. Fig. 4 shows the comparison of the average PCM temperature during solidification between the current model and the experimental data. The close agreement demonstrates the ability of the numerical model to accurately predict the thermal performance of PCM-based systems. This provides confidence in utilizing the model to gain insights into the impacts of different parameters on PCM solidification behavior. This validation confirms the model reliably to gain insights into the impacts of different parameters on PCM discharge behavior in triplex-tube systems.

5. Results and discussions

This section presents the results of the comprehensive investigation conducted to explore the impacts of various design parameters and operating conditions on the solidification rates and kinetics of PCMs within a zigzag-shaped triplex-tube heat exchanger. The effects of geometric modifications, including variations in the zigzag angle and length, are systematically analyzed to identify optimal

Table 2
Impact of grid number and time step size on the charging period.

Number of cells	172016	267002			419903
Time step size (s)	0.2	0.1	0.2	0.4	0.2
Discharge rate (W)	40.62	41.44	41.38	41.18	41.45

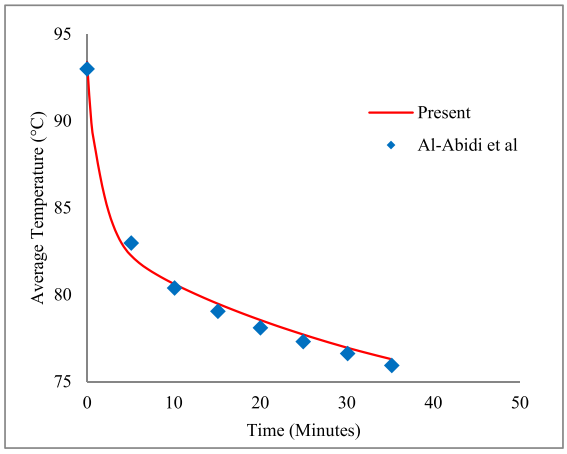

Fig. 4. The change in PCM temperature over time during the melting process is depicted for both the numerical model employed in the present study and the experimental data reported by Al-Abidi et al. [49].

configurations that enhance heat transfer and accelerate solidification. Furthermore, the influence of flow conditions, such as the Reynolds number and inlet temperature of the HTF, on the solidification process is evaluated. Additionally, the potential of incorporating nanoparticle additives into the PCM to improve its thermal properties and solidification characteristics is explored. Through a detailed analysis of the liquid fraction, temperature profiles, and solidification rates, key insights are provided into the intricate interplay between these parameters and their impact on the overall solidification performance of the LHTES system.

5.1. Geometry modification

5.1.1. Effect of the zigzag degree

The solidification of PCMs is a complex phenomenon involving the intricate interplay of heat transfer, fluid dynamics, and phase transition behaviors. In order to gain insights into how the geometry of the heat exchanger tubes influences this process, this study conducted an in-depth analysis of the PCM solidification profiles for various zigzag tube configurations and compared them against a straight tube baseline case. Figs. 5 and 6 present the transient contour plots for the liquid fraction and temperature evolution during the solidification of PCM for various zigzag geometries, including Case 0 with a zigzag angle (0°) and Cases 1,2,and 3 with zigzag angles of 22.5°, 45°, and 67.5°, respectively. The analysis of these figures reveals the intricate interplay between the zigzag geometry and the heat transfer mechanisms governing the solidification kinetics.

In Fig. 5, the liquid-fraction contour exhibit a clear decreasing trend with increasing time, reflecting the progressive solidification of the PCM. However, the rate of this decrease is significantly influenced by the zigzag angle. At 2400 s, the straight channel case (Case 0) maintains a liquid fraction of approximately 0.75, indicating that a substantial portion (75 %) of the PCM remains in the liquid phase. In contrast, the introduction of zigzag angles substantially accelerates the solidification rate, as evidenced by the lower liquid fractions of 0.87, 0.79, and 0.67 for the cases 1–3 with 22.5°, 45°, and 67.5° zigzag angles, respectively. These quantitative differences in liquid fraction can be attributed to the enhanced heat transfer mechanisms facilitated by the zigzag geometries. Specifically, the zigzag configuration increases the effective heat transfer surface area between the PCM and the HTF, enabling more efficient extraction of thermal energy from the PCM. Additionally, the sharp bends in the zigzag geometry promote the formation of vortices and complex flow patterns within the PCM domain, which further augment convective heat transfer and mixing, thereby accelerating the solidification process.

The temperature contours in Fig. 6 corroborate the observations from the liquid fraction data and provide deeper insights into the underlying heat transfer mechanisms. At 2400 s, the straight channel case exhibits an average PCM temperature of approximately 47 °C, indicating that a significant portion of the PCM remains in the liquid phase and has not yet released its latent heat of solidification. Conversely, the zigzag cases exhibit lower average temperatures of approximately 43 °C, 38 °C, and 33 °C for the cases 1–3 with 22.5°, 45°, and 67.5° angles, respectively, at the same time step. These lower temperatures in the zigzag cases can be directly attributed to the increased heat transfer rates facilitated by the enlarged surface area and vortex-induced mixing. As the PCM solidifies, it releases its latent heat of fusion, resulting in a temperature decrease. The more rapid temperature drop observed in the zigzag cases, particularly the 67.5° configuration, indicates a faster release of latent heat and a more advanced stage of solidification compared to the straight channel case. Notably, the 67.5° zigzag angle emerges as the optimal configuration, exhibiting the lowest liquid fraction of 0.67 and the lowest average temperature of 33 °C at 2400 s. This superior performance can be attributed to the synergistic effects of maximized heat transfer surface area and enhanced vortex formation at this high zigzag angle, which collectively facilitate more efficient heat extraction from the PCM and accelerate the solidification process.

Fig. 7 presents the stream vector visualization of the HTF flow patterns for different time steps across the various zigzag angle cases, including Case 0 with straight channel (0°-zigzag angle) and Cases 1–3 with zigzag angles of 22.5°, 45°, and 67.5°, respectively. In the straight channel case (Case 0), the stream vectors exhibit a parallel and uniform flow pattern, which is characteristic of laminar flow in

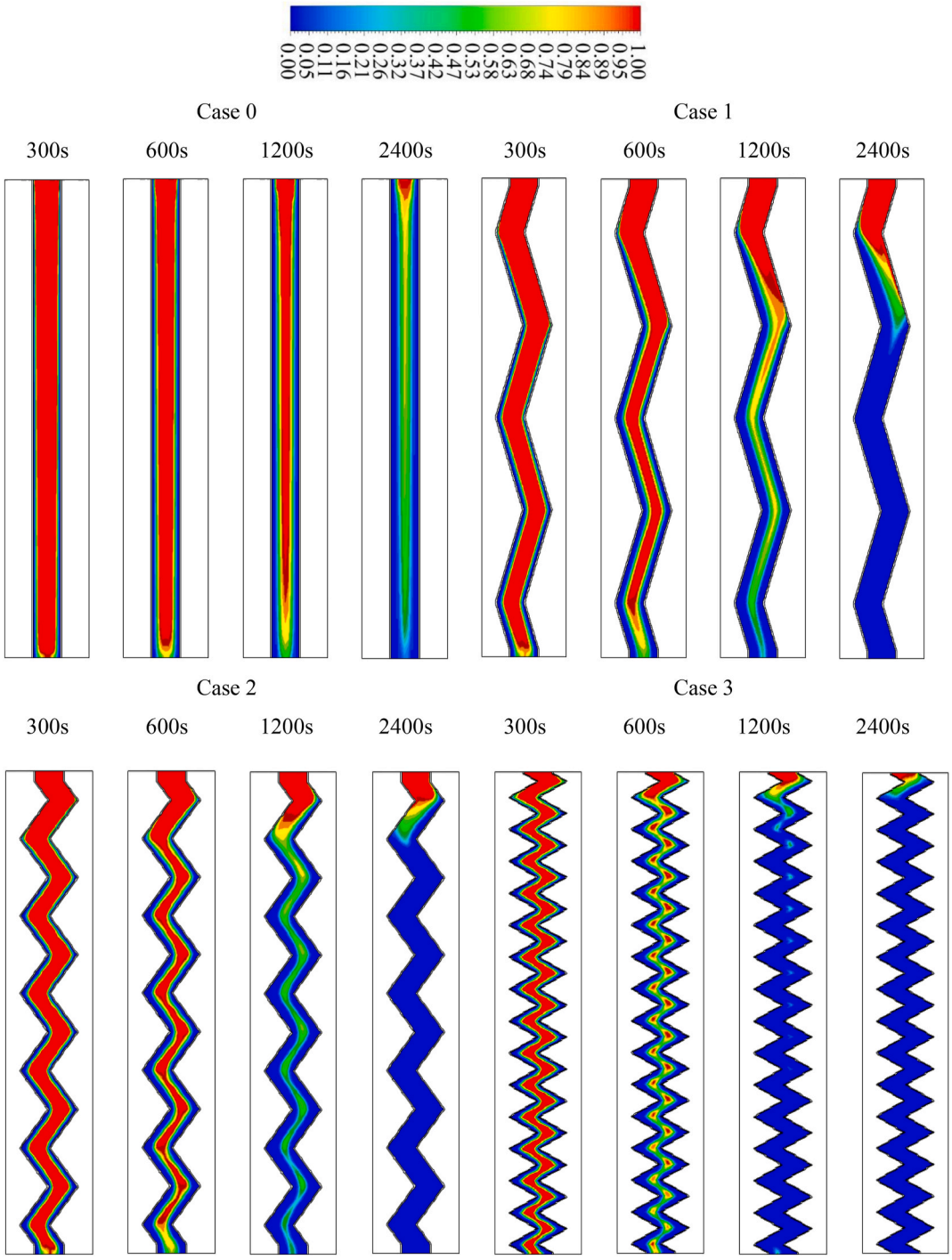

Fig. 5. Liquid fraction development for different time steps for the cases of the straight channel and various zigzag angles.

straight channels. The absence of any geometric obstructions or deviations results in a streamlined flow without any significant vortex formation or mixing. This laminar flow pattern is less conducive to enhancing convective heat transfer, which can lead to slower solidification rates, as observed in the liquid fraction and temperature data presented in Figs. 5 and 6.

In contrast, the introduction of zigzag angles in Cases 1–3 significantly alters the flow patterns, leading to the formation of vortices and complex fluid dynamics. At a zigzag angle of 22.5°, the stream vectors begin to deviate from the parallel flow pattern, with slight vortex formations observed in the vicinity of the zigzag bends. As the zigzag angle increases to 45°, the vortex formations become more pronounced, with larger swirling flow patterns evident in the regions between the zigzag elements. The most prominent vortex

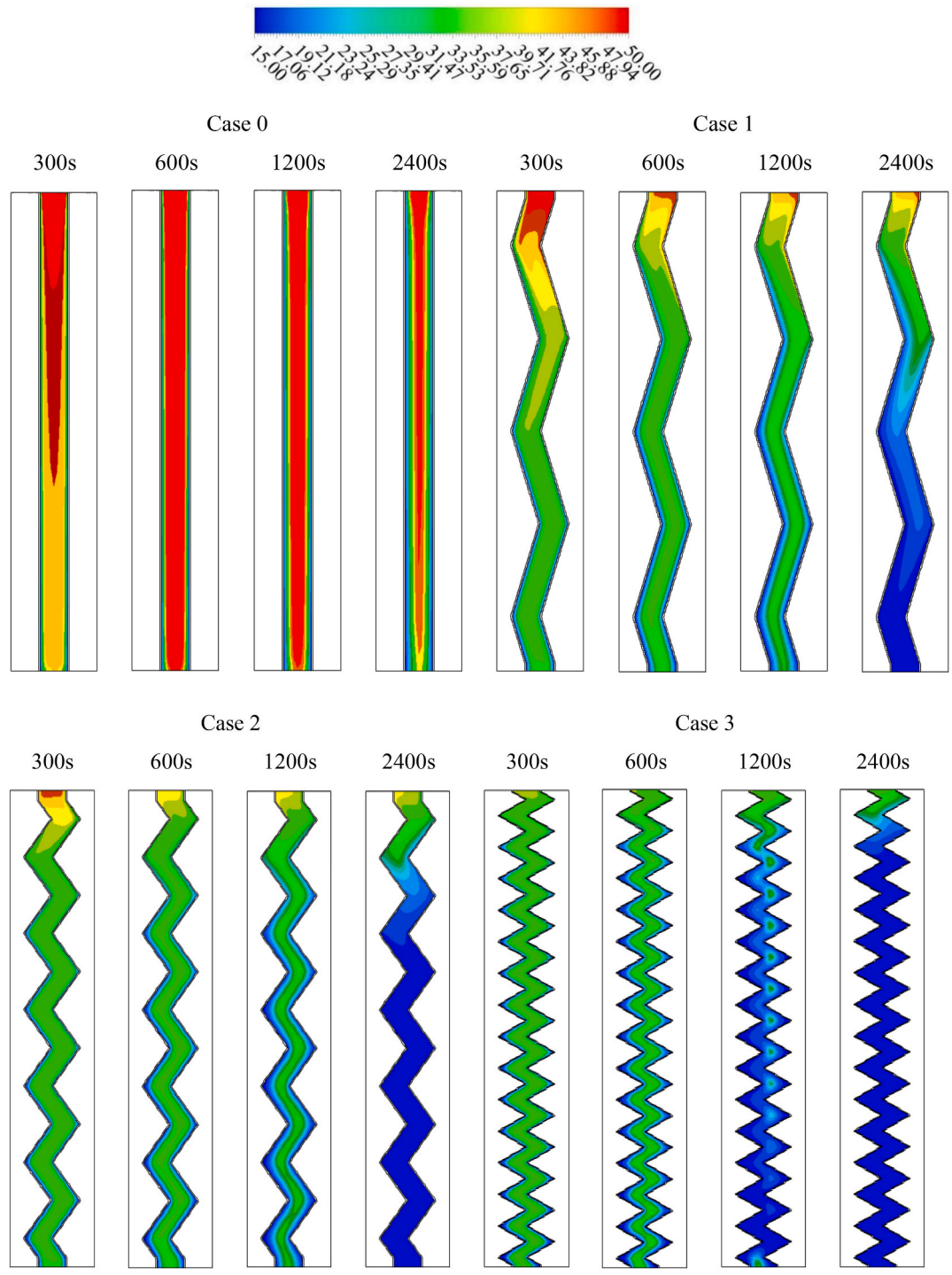

Fig. 6. Average temperature development for different time steps for the cases of the straight channel and various zigzag angles.

formations are observed in the 67.5° zigzag angle case, where the stream vectors exhibit distinct swirling patterns within each zigzag element. These vortices are generated due to the sharp turns and abrupt changes in flow direction imposed by the high zigzag angle, causing the fluid to rotate and mix within the confined spaces between the zigzag elements. This observation aligns with the liquid fraction and temperature data presented in Figs. 5 and 6, where the 67.5° zigzag angle case exhibited the fastest solidification rates and the lowest liquid fractions and temperatures at any given time step. The analysis of vector plots in Fig. 7 reveals the significant impact of the zigzag geometry on the fluid flow patterns within the system. The introduction of zigzag configuration promotes the formation of

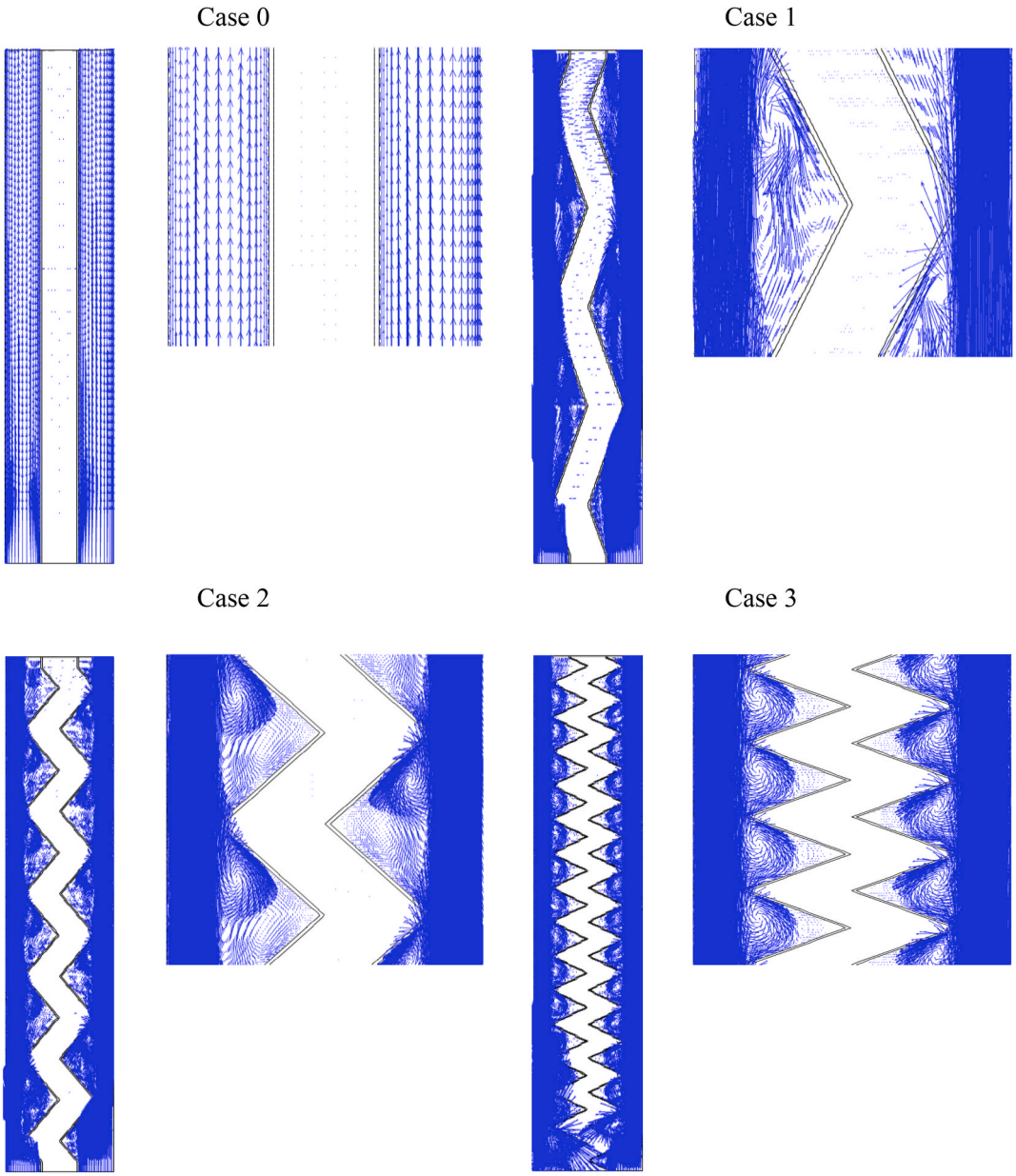

Fig. 7. Stream vector for different time steps for the cases of the straight channel and various zigzag angles.

vortices and complex fluid dynamics, which can enhance the convective heat transfer between the HTF and the PCM. Furthermore, the liquid fraction and temperature contour plots presented in Figs. 5 and 6 confirm the positive impact of the zigzag geometry on the PCM solidification kinetics. These plots show that the zigzag configuration, particularly at higher angles, can significantly accelerate the solidification process by facilitating more efficient heat extraction from the PCM.

The transient evolution of the average PCM temperature and liquid-fraction profiles is illustrated in Figs. 8 and 9, respectively. The data presented in these figures reveal a clear trend of lower average temperature and smaller liquid fraction values with increasing zigzag angles. The superior solidification performance of higher zigzag angles is further evidenced by the results summarized in Table 2. The data shows a clear trend of faster solidification rates and reduced total solidification times with increasing zigzag angle. Among all the angles examined, the 67.5° configuration displays the best discharge characteristics based on the liquid fraction profiles, average temperature profiles, and overall solidification duration. As noted in the data, 95 % of the PCM solidifies within 1200 s, and the whole PCM reaches thermal equilibrium within 1400 s. Generally, the PCM temperature and liquid-fraction profiles analysis highlights the important role that the zigzag angle plays in determining the transient evolution of solidification in phase change systems. The data suggest that higher zigzag angles result in faster solidification rates and shorter solidification durations, with the

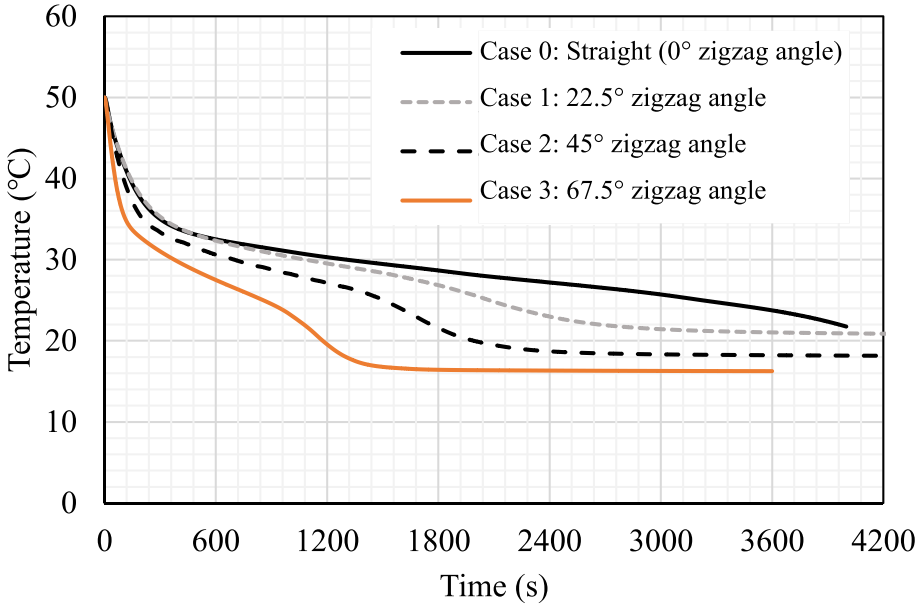

Fig. 8. Average temperature profile for different time steps for the cases of the straight channel and various zigzag angles.

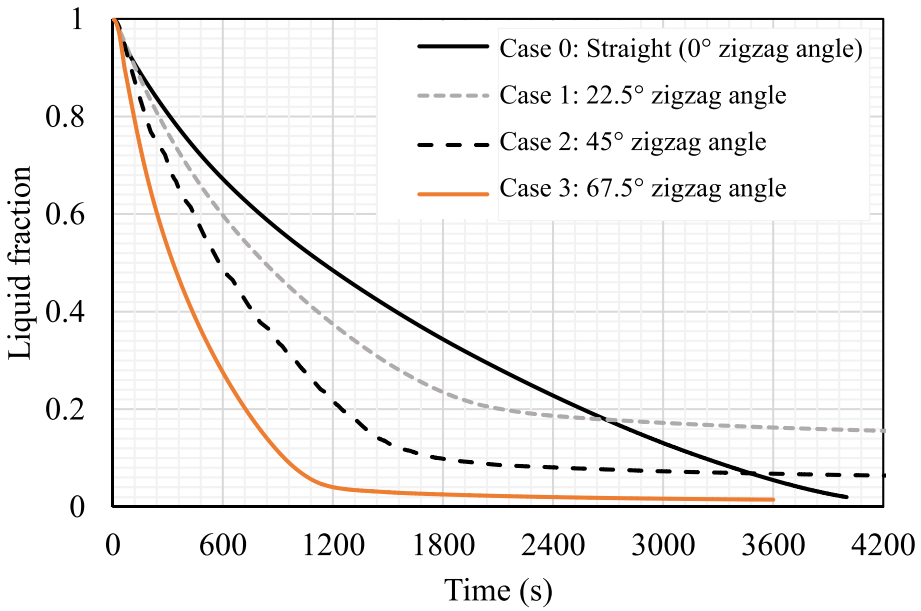

Fig. 9. Liquid fraction profile for different time steps for the cases of the straight channel and various zigzag angles.

Table 3
The solidification rate and the liquid fraction after 3600s for the cases of the straight channel and various zigzag angles.

Studied model	Solidification rate (W)	Liquid fraction after 3600s
Straight channel (Case 0)	39.63	0.055
22.5°- channel (Case 2)	37.34	0.163
45°- channel (Case 3)	41.38	0.068
67.5°- channel (Case 4)	43.8	0.015

67.5° zigzag angle demonstrating exceptional discharge performance.

Table 3 presents quantitative data on the solidification rate and the liquid fraction of the phase change material (PCM) after 3600 s for different zigzag angle configurations, including the straight channel of 0°-zigzag angle (Case 0) and Cases 1–3 with zigzag angles of 22.5°, 45°, and 67.5°, respectively °. The straight channel case exhibits a solidification rate of 39.63 W, which serves as the baseline for comparison. When a zigzag angle of 22.5° is introduced, the solidification rate decreases to 37.34 W, representing a reduction of about 5.8 % compared to the straight channel configuration. This decrease in solidification rate can be attributed to the relatively low zigzag angle, which may not provide sufficient enhancement in heat transfer surface area and vortex formation to overcome the increased flow resistance and pressure drop associated with the zigzag geometry. As the zigzag angle increases to 45°, the solidification rate improves to 41.38 W, surpassing the straight channel case by about 4.4 %. This improvement can be attributed to the larger heat transfer surface area and more pronounced vortex formations facilitated by the higher zigzag angle, which enhance convective heat transfer and accelerate the solidification process. The 67.5° zigzag angle case exhibits the highest solidification rate of 43.8 W, outperforming the straight channel by 10.6 %, the 22.5° case by 17.3 %, and the 45° case by 5.8 %. This superior performance can be attributed to the synergistic effects of maximized heat transfer surface area and enhanced vortex formation at this high zigzag angle, which collectively facilitate more efficient heat extraction from the PCM and accelerate the solidification process.

The liquid fraction data further corroborates the solidification rate findings. The straight channel case exhibits a liquid fraction of 0.055, indicating that a small portion (5.5 %) of the PCM remains in the liquid phase after 3600 s. The 22.5° zigzag angle case displays the highest liquid fraction of 0.163, suggesting that a significant portion (16.3 %) of the PCM remains unsolidified at this time step. In contrast, the 45° zigzag angle case exhibits a liquid fraction of 0.068, lower than the straight channel case, indicating more effective solidification. The 67.5° zigzag angle case outperforms all other configurations with the lowest liquid fraction of 0.015, signifying that only 1.5 % of the PCM remains in the liquid phase after 3600 s. In summury, the data presented in Table 3 clearly demonstrates the profound impact of the zigzag angle on the solidification performance of the PCM. The introduction of higher zigzag angles, particularly the 67.5° configuration, leads to substantial improvements in solidification rate and reductions in liquid fraction compared to the straight channel and lower angle cases.

5.1.2. Effect of the zigzag length variations

Figs. 10 and 11 present the analysis of the impact of varying the zigzag length on the solidification behavior of the PCM in charge. The figures depict the contour plots for the tranient liquid fraction and temperature evolution, respectively, for different zigzag lengths of H = 5 mm, 10 mm, and 15 mm, while maintaining a constant zigzag angle of 67.5°. The analysis of these figures reveals valuable insights into the influence of the zigzag length on the solidification kinetics. At the initial time step of 300 s, all three cases in Fig. 10 exhibit a liquid fraction of 1, indicating that the PCM is entirely in the liquid phase. As time progresses, the liquid fraction decreases across all cases, signifying the progression of solidification. However, the rate of this decrease varies significantly based on the zigzag

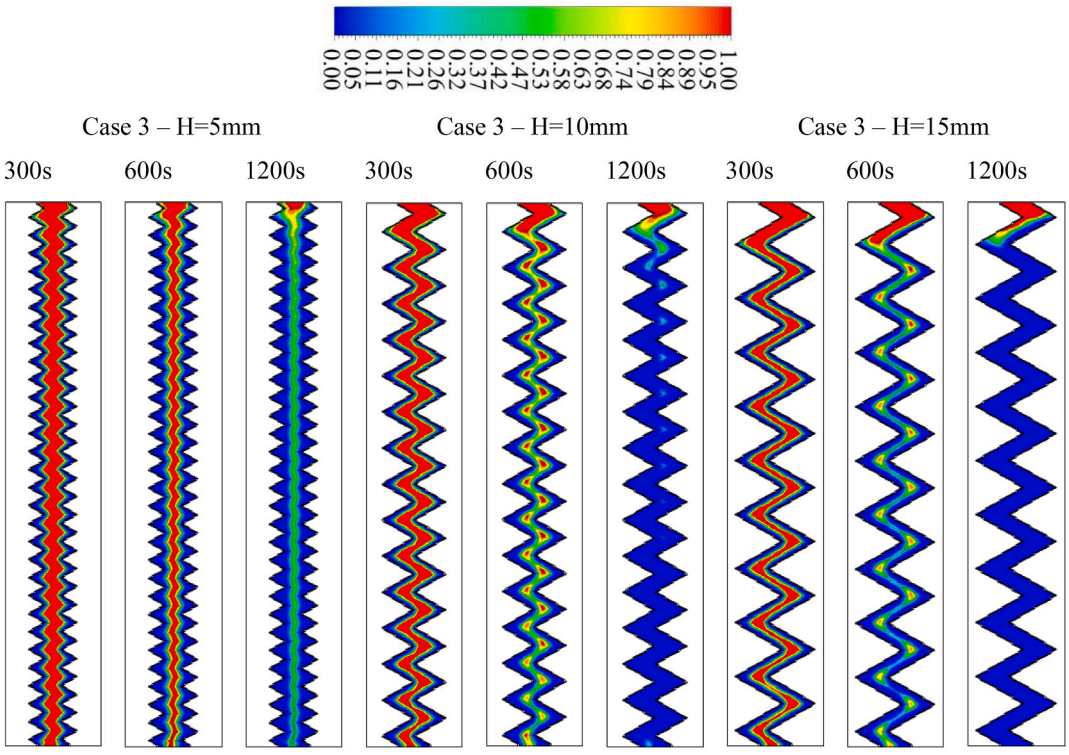

Fig. 10. Liquid fraction development for different time steps for the cases of various zigzag lengths.

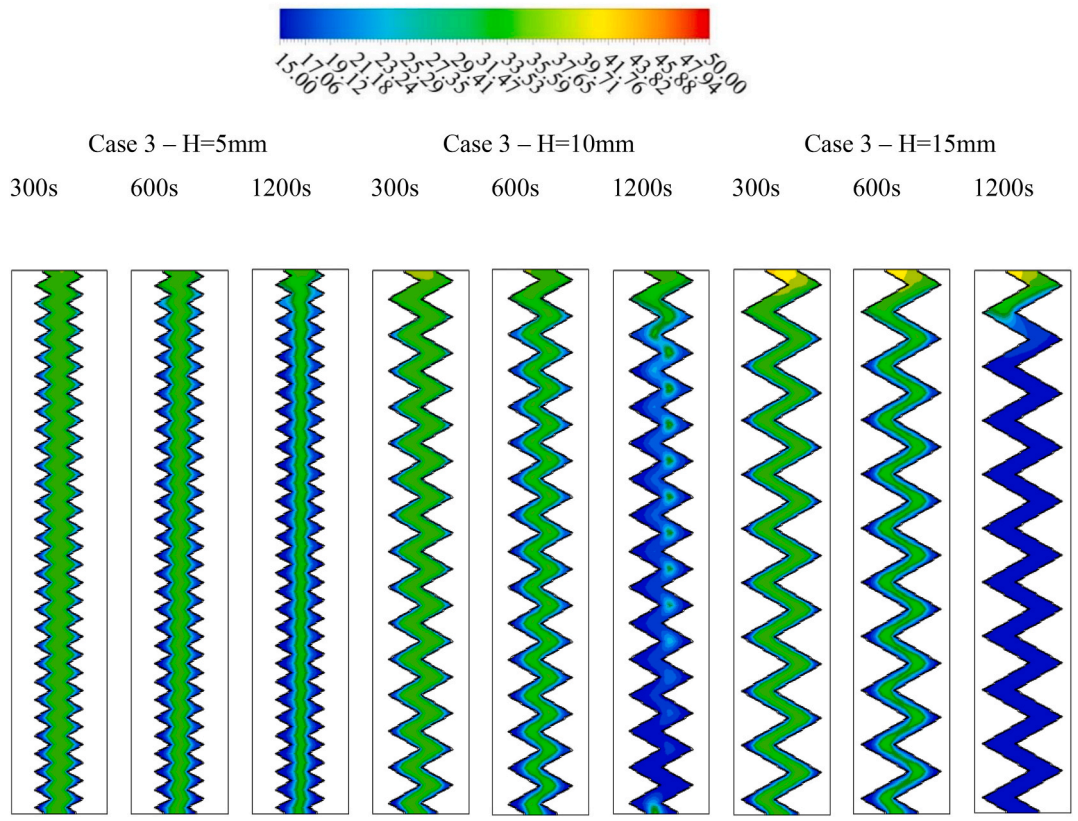

Fig. 11. Temperature development for different time steps for the cases of various zigzag lengths.

length. The case with a 15 mm zigzag length exhibits the fastest solidification rate, as evidenced by the steepest decline in the liquid fraction profile. By the 1200-s mark, the liquid fraction has decreased to approximately 0.3 for the 15 mm case, while the 10 mm and 5 mm cases maintain higher liquid fractions of around 0.5 and 0.65, respectively. This trend suggests that increasing the zigzag length leads to an acceleration of the solidification process, with the 15 mm case solidifying most rapidly.

The temperature contour plots in Fig. 11 further corroborate the observations from the liquid fraction data. At 300 s, all cases exhibit a uniform temperature distribution within the PCM domain, reflecting the initial liquid state. As time progresses, localized temperature gradients become apparent, particularly near the zigzag walls, indicating the progression of solidification. The temperature contours reveal that the 15 mm zigzag length case exhibits the fastest cooling and solidification, with larger regions of the PCM domain reaching lower temperatures more rapidly compared to the 10 mm and 5 mm cases. This accelerated cooling is directly attributed to the increased heat transfer surface area provided by the longer zigzag length, which facilitates more efficient heat extraction from the PCM. Overall, the data presented in Figs. 10 and 11 show that by extending the zigzag length from 5 mm to 15 mm, the time required for 95 % solidification of the PCM decreases from 1530 s to 948 s, representing a substantial 61.5 % reduction in

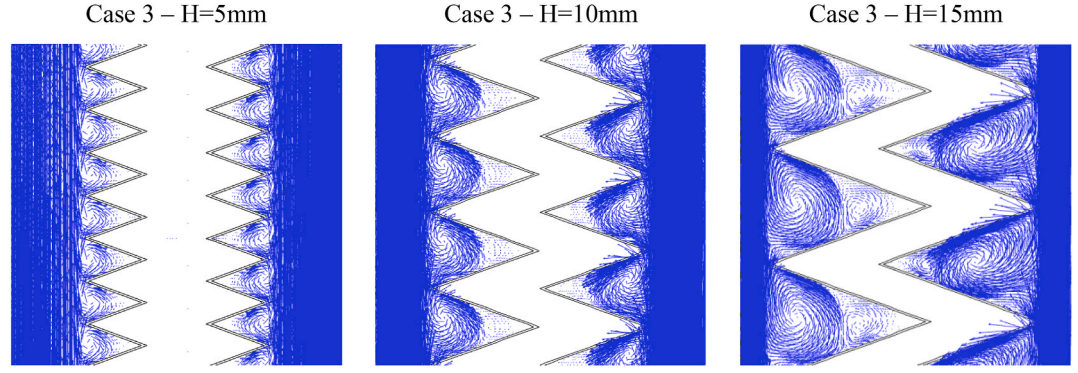

Fig. 12. Stream vector for case with different zigzag lengths at t = 1200s.

solidification time. This improvement can be attributed to the larger heat transfer surface area offered by the longer zigzag length, enabling more effective heat extraction from the PCM and driving faster solidification kinetics. The temperature contour plots further reinforce this observation, with the 15 mm case exhibiting more rapid cooling and larger regions of solidified PCM within the same time frame compared to the shorter zigzag length cases.

Fig. 12 provides a visual representation of the flow patterns of the HTF within the zigzag channel for different zigzag lengths of H = 5 mm, 10 mm, and 15 mm at a specific time step of 1200 s. The stream vector plots offer valuable insights into the influence of the zigzag length on the fluid dynamics and heat transfer characteristics of the system. For the case with H = 5 mm zigzag length, the stream vectors exhibit a relatively simple flow pattern. The fluid flow is predominantly parallel to the channel walls, with minor deviations and vortex formations observed in the vicinity of the zigzag bends. These vortices are relatively small in size and localized, indicating that the fluid mixing and heat transfer enhancement effects are limited in this configuration. As the zigzag length increases to 10 mm, the stream vector plots reveal more pronounced vortex formations within the confined spaces between the zigzag elements. These vortices are larger in size and occupy a substantial portion of the channel cross-section, suggesting increased fluid mixing and turbulence. The presence of these vortices can potentially enhance the convective heat transfer between the HTF and the PCM, contributing to improved solidification rates. The most significant vortex formations are observed in the case with a zigzag length of H = 15 mm. In this configuration, distinct and sizable vortices are formed within each zigzag element, occupying a substantial portion of the channel's cross-sectional area. Furthermore, the stream vectors indicate the presence of double swirls within each confined zigzag zone, indicating complex fluid dynamics and enhanced mixing. These double swirls can effectively disrupt the boundary layer formation along the channel walls, leading to increased heat transfer rates between the HTF and the PCM.

Figs. 13 and 14 depict the liquid fraction and average temperature profiles, respectively, for different zigzag lengths (H = 5 mm, 10 mm, and 15 mm) during the solidification mode of the PCM. In Fig. 13, the liquid fraction curves exhibit a decreasing trend over time, indicating the progressive solidification of the PCM. However, the rate of this decrease is significantly influenced by the zigzag length. The case with a zigzag length of 15 mm demonstrates the fastest solidification rate, reaching a liquid fraction of 0.05 (95 % solidification) within only 948 s. In contrast, the cases with zigzag lengths of 10 mm and 5 mm take considerably longer times of 1115 s and 1531 s, respectively, to achieve the same liquid fraction of 0.05. Furthermore, the liquid fraction curves reveal that after reaching the 95 % solidification mark, the rate of decrease slows down considerably for all cases. This behavior can be attributed to the confinement of the remaining liquid fraction at the top of the domain, where the temperature difference between the PCM and the HTF is reduced, leading to a lower heat transfer rate and slower solidification of the remaining liquid PCM.

Fig. 14 presents the average temperature profiles of the PCM for the different zigzag lengths. Initially, all cases exhibit a rapid temperature drop within the first 100 s, which can be attributed to the high temperature difference between the PCM and the HTF, resulting in a high convective heat transfer rate. However, as the solidification process progresses, the temperature profiles diverge based on the zigzag length. The case with a 15 mm zigzag length exhibits the fastest temperature reduction, reaching thermal equilibrium at approximately 16 °C within 948 s. In contrast, the cases with 10 mm and 5 mm zigzag lengths take longer times of 1115 s and 1531 s, respectively, to reach the same equilibrium temperature. It is noteworthy that the equilibrium temperature of 16 °C is slightly higher than the inlet temperature of the HTF (15 °C). This difference can be attributed to the presence of a small liquid fraction (approximately 5 %) remaining at the top of the domain, even after the solidification process is completed. This residual liquid fraction acts as an insulating layer, resulting in a slightly higher equilibrium temperature within the PCM domain.

Table 4 compares quantativly the performance of three three cases: Case 3 with a zigzag length of 5 mm, Case 3 with a zigzag length of 10 mm, and Case 3 with a zigzag length of 15 mm. The data in this table shows a clear trend of increasing solidification rate and

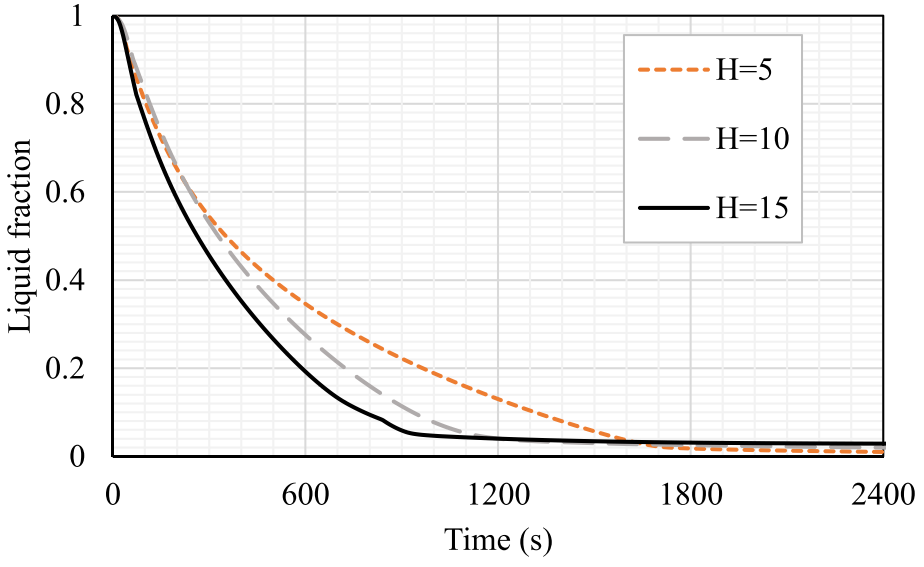

Fig. 13. Liquid fraction profile for different time steps for the various zigzag lengths.

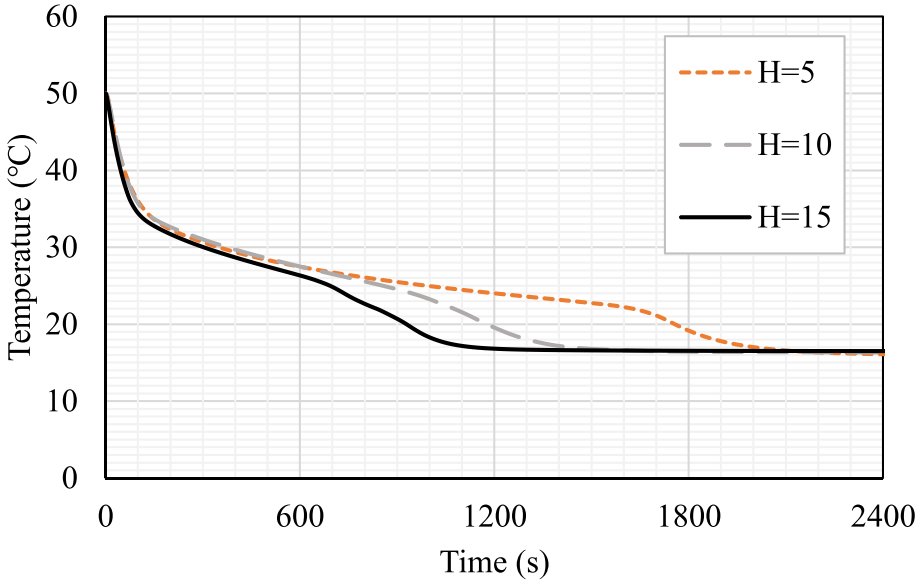

Fig. 14. Average temperature profile for different time steps for the various zigzag lengths.

Table 4
The solidification rate and time for various zigzag lengths.

Studied model	Solidification rate (W)	Solidification time (s)
Case 3 (H = 5 mm)	94.57	1531
Case 3 (H = 10 mm)	131.55	1115
Case 3 (H = 15 mm)	157.38	948

decreasing solidification time as the zigzag length increases. The case with a zigzag length of 5 mm exhibits the lowest solidification rate of 94.57 W and the longest solidification time of 1531 s. When the zigzag length is increased to 10 mm, the solidification rate improves to 131.55 W, representing a 39.1 % increase compared to the 5 mm case. Correspondingly, the solidification time decreases to 1115 s, a reduction of 27.2 % compared to the 5 mm case. This improvement in performance can be attributed to the larger heat

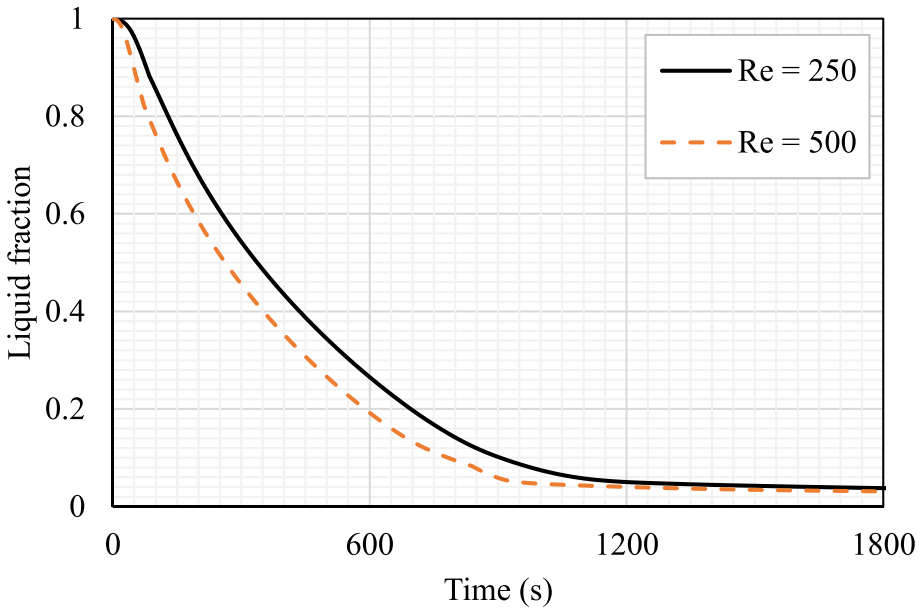

Fig. 15. Liquid fraction profile for different time steps for the various Re (250 and 500).

transfer surface area provided by the longer 10 mm zigzag length, enabling more efficient heat extraction from the PCM and accelerating the solidification process.

The case with a zigzag length of 15 mm exhibits the highest solidification rate of 157.38 W and the shortest solidification time of 948 s. Compared to the 5 mm case, the solidification rate is 66.5 % higher, and the solidification time is 38.1 % shorter. Even when compared to the 10 mm case, the 15 mm zigzag length offers a 19.7 % higher solidification rate and a 15 % reduction in solidification time. These substantial improvements can be attributed to the further increase in heat transfer surface area provided by the extended 15 mm zigzag length, facilitating even more efficient heat exchange between the PCM and the HTF.

These quantitative improvements in solidification rate and time can be directly attributed to the increased heat transfer surface area provided by the longer zigzag lengths. The larger surface area facilitates more efficient heat extraction from the PCM, driving faster solidification kinetics and reducing the overall solidification time. The results highlight the importance of optimizing the zigzag length in PCM containment systems to achieve desired solidification performance and efficient thermal energy storage and release.

5.2. HTF flow conditions

5.2.1. Effect of the HTF Reynolds number

The figures in this section present the results of an investigation into the impact of Reynolds number (Re) on the solidification rate of the PCM in a zigzag element system. The angle and length of the zigzag element were fixed at 67.5° and 15 mm, respectively. At the same time, two different Reynolds numbers, 500 and 250, were considered to examine the effect of flow rate on the PCM's solidification rate. Fig. 15 indicate that a higher Reynolds number, which corresponds to a higher flow rate of the HTF, leads to a faster solidification rate of the PCM. This is because a higher flow rate provides a fresh coolant to the system, which maintains a higher temperature difference between the coolant and the PCM, thereby accelerating the solidification process. The results of Fig. 16 further highlight the relationship between the flow rate and the solidification rate of the PCM, showing that the HTF's flow rate influences the PCM's average temperature. Because of the higher temperature difference between the HTF and the PCM in the case of the higher Re, the average temperature of the PCM drops to the 16 °C by 948 s in the case of Re equal 500, and by 1204 s for the case of Re equal 250.

While these results provide important insights into the role of Reynolds number and flow rate in the solidification rate of PCM systems, it is essential to note that the study only considers two specific Reynolds numbers and does not consider other variables that may impact the PCM's solidification rate. For instance, the type of PCM, the geometry of the system, and the temperature of the HTF are essential factors that can impact the temperature and solidification rate of the PCM and should be considered in future studies.

Based on the data provided, it appears that the solidification rate and time of the PCM are being affected by the Reynolds number (Re) (Table 5). When the Reynolds number is 250, the solidification rate of the PCM is 125.1 W, and the solidification time is 1204 s. When the Reynolds number is increased to 500, the solidification rate increases to 157.4 W, and the solidification time decreases to 948 s. This indicates that as the Reynolds number increases, the solidification rate of the PCM also increases, and the solidification time decreases. This can be due to the increase in the flow velocity of the fluid, which causes the heat transfer to be more efficient and leads to a faster solidification time and higher solidification rate. However, to further analyze the relationship between the Reynolds number, solidification rate, and solidification time, additional information such as the fluid's temperature, the PCM's properties, and the system's geometry is necessary. The relationship between these variables can be complex and influenced by multiple factors, and a

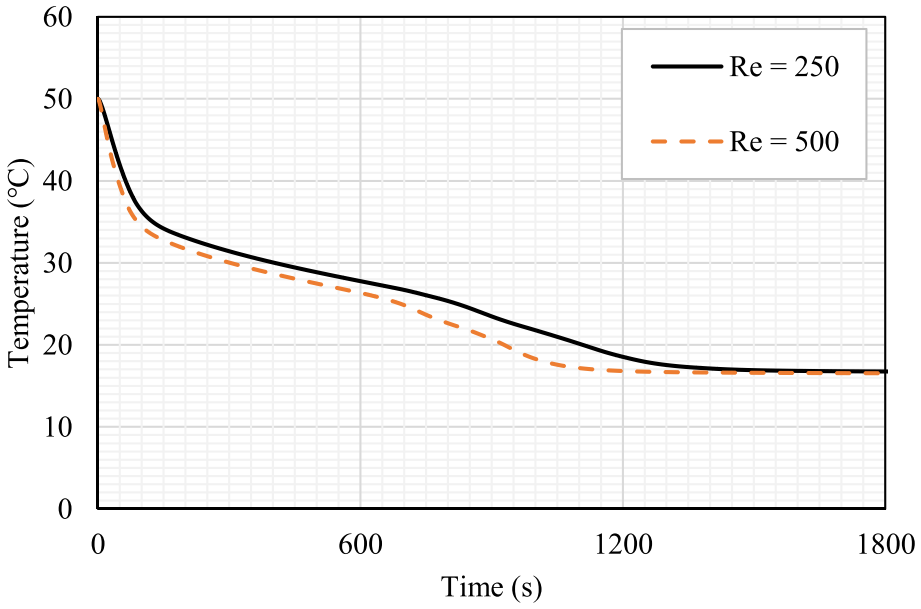

Fig. 16. The temperature profile for different time steps for the various Re (250 and 500).

Table 5
The solidification rate and time for various Re (250 and 500) for Case 3 of H = 15 mm.

Studied model	Solidification rate (W)	solidification time (s)
Reynolds = 250	125.1	1204
Reynolds = 500	157.4	948

thorough analysis would require a more detailed understanding of the system.

5.2.2. Effect of the HTF temperature

The inlet temperature of the HTF has a significant impact on the PCM solidification rate and duration. As depicted in Fig. 17, increasing the temperature difference between the HTF and PCM leads to accelerated solidification. This is attributed to the higher heat release rate from the PCM to the colder HTF, which is proportional to the temperature gradient. A large temperature difference causes rapid solidification of most of the PCM, however a small fraction (5 %) remains liquid at the top, extending the total time. Fig. 18 further demonstrates faster reductions in the average PCM temperature for lower HTF inlet temperatures, owing to the enhanced heat transfer rate. Nevertheless, while HTF inlet temperature is a critical factor, other parameters also govern PCM solidification, including the thermophysical properties, geometry, and HTF flow characteristics. This study elucidates the complex relationship between HTF inlet temperature and PCM freezing behavior. The insights gained can guide design optimization of PCM-based heat exchangers to leverage HTF inlet temperature control for accelerated solidification.

The inlet temperature of the HTF significantly impacts the solidification rate and time of the PCM. The temperature difference between the PCM and the HTF affects the heat transfer rate, which influences the solidification rate and time of the PCM, as shown in Table 6. When the inlet temperature of the HTF is 10 °C, the solidification rate of the PCM is 198.4 W, and the solidification time is 774 s. When the inlet temperature of the HTF is increased to 15 °C, the solidification rate decreases to 157.4 W, and the solidification time increases to 948 s. This suggests that as the inlet temperature of the HTF increases, the temperature difference between the PCM and the HTF decreases, resulting in a lower heat transfer rate and a slower solidification process. However, when the inlet temperature of the HTF is further increased to 20 °C, the temperature difference between the PCM and the coolant is reduced even more, causing a lower solidification rate of 74.9 W and a longer solidification time of 1956 s. This indicates that a high inlet temperature of the HTF can have a detrimental effect on the solidification process, as the temperature difference between the PCM and the HTF is insufficient to drive an efficient heat transfer process. It is important to note that the inlet temperature of the HTF is not the only factor affecting the solidification rate and time of the PCM. Other factors, such as the properties of the PCM, the flow characteristics of the HTF, and the geometry, also play essential roles in determining the solidification process.

5.3. Impact of nanoadditive incorporation

The incorporation of nanoparticles into PCMs is a promising approach to enhance their thermal conductivity and heat transfer characteristics, thereby improving the overall solidification performance in LHTES systems. In this section, the influence of various

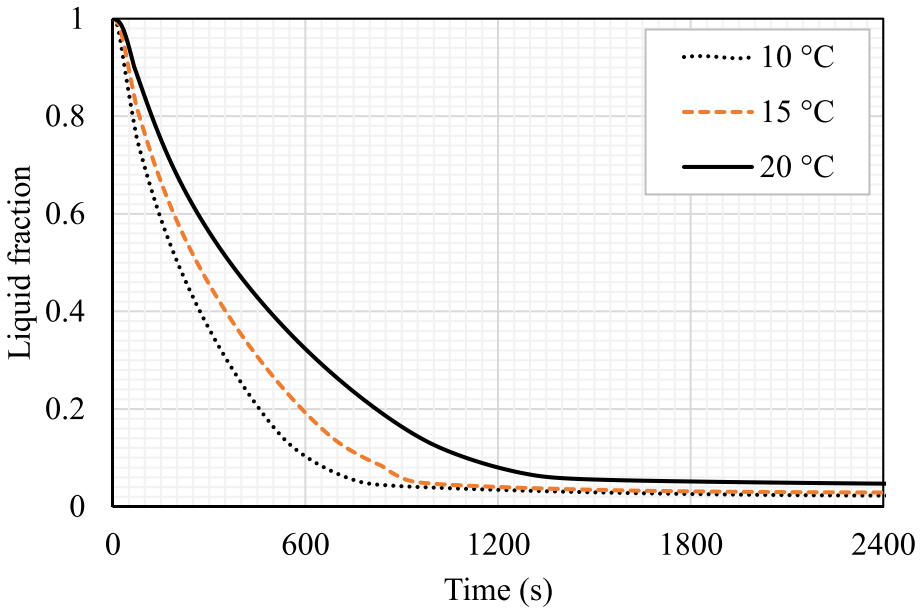

Fig. 17. Liquid fraction profile for different time steps for the various inlet temperature of the HTF.

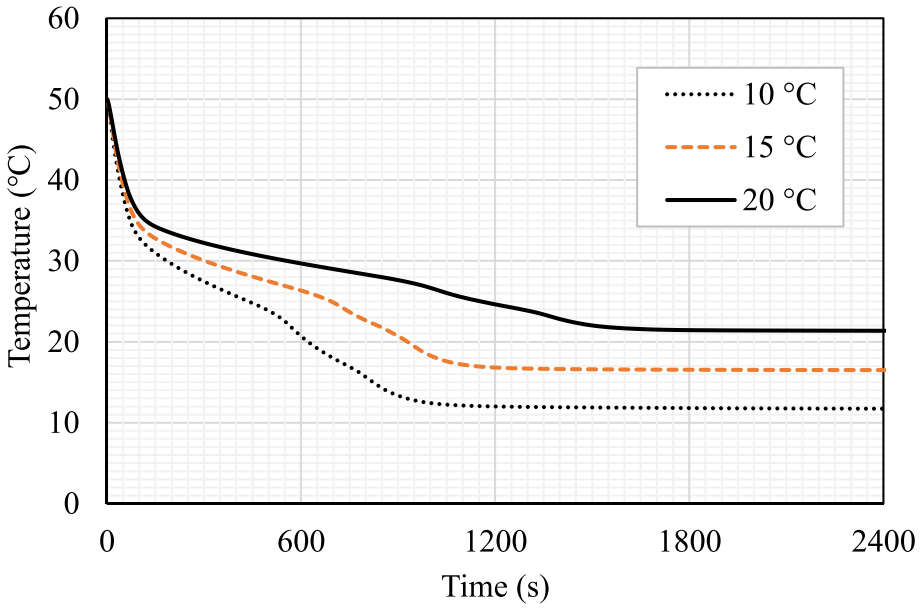

Fig. 18. The temperature profile for different time steps for the various inlet temperature of the HTF.

Table 6
The solidification rate and time for different time steps for the various inlet temperature of the HTF for Case 3 of H = 15 mm.

Studied model	Solidification rate (W)	Solidification time (s)
HTF Temperature = 10 °C	198.4	774
HTF Temperature = 15 °C	157.4	948
HTF Temperature = 20 °C	74.9	1956

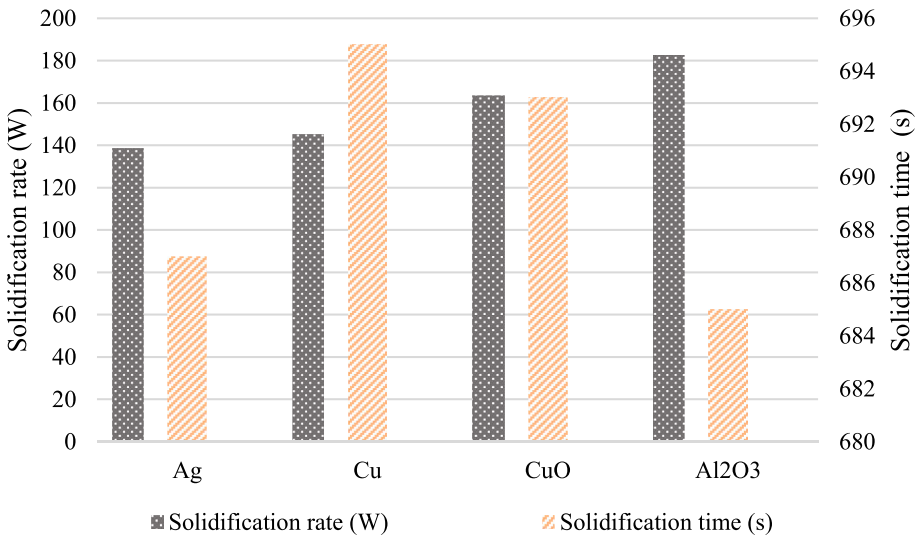

Fig. 19. The solidification rate and time for different types of nanoparticles mixed with the PCM.

nanoparticle types (Al_2O_3, CuO, Cu, Ag) and concentrations (2–6 % v/v) on the solidification rates and durations of the PCM was systematically investigated. Fig. 19 illustrates the solidification rate and time for the PCM when dispersed with different nanoparticle additives. The results indicate that the addition of nanoparticles can substantially increase the solidification rate compared to the baseline case of pure PCM, with Al_2O_3 nanoparticles exhibiting the most favorable performance enhancement. Specifically, the

incorporation of 4 % Al_2O_3 nanoparticles led to a 16 % increase in solidification rate, from 157.4 W for pure PCM to 182 W for the Al_2O_3-PCM nanocomposite. This augmentation in solidification rate can be attributed to the high thermal conductivity of Al_2O_3 (37 W/m-K), which facilitates more efficient heat extraction from the PCM during the phase change process. Furthermore, the solidification time was also found to be inversely related to the nanoparticle loading concentration. While the solidification duration for pure PCM was 948 s, the addition of 4 % Al_2O_3 nanoparticles reduced this time to 685 s, representing a substantial 38 % reduction. This decrease in solidification time can be attributed to the combined effects of enhanced thermal conductivity and increased heat capacity provided by the Al_2O_3 nanoparticles, which accelerate the heat transfer and phase transition kinetics within the PCM.

To further elucidate the influence of nanoparticle concentration, Fig. 20 presents the solidification rate and time for the PCM with varying concentrations (2 %, 4 %, and 6 %) of Al_2O_3 nanoparticles. The results demonstrate a clear trend of increasing solidification rate and decreasing solidification time with higher nanoparticle concentrations. Compared to pure PCM, the incorporation of 2 %, 4 %, and 6 % Al_2O_3 nanoparticles led to solidification rate enhancements of 9.6 %, 11.4 %, and 11.5 %, respectively. Similarly, the solidification times were reduced from 948 s for pure PCM to 734 s, 685 s, and 652 s for the 2 %, 4 %, and 6 % Al_2O_3-PCM nanocomposites, respectively.

It is important to note that the specific configurations tested in this study were carefully chosen to capture the key physical mechanisms governing phase change heat transfer in a zigzag-shaped triplex-tube LHTES system. The tested parameters, including variations in zigzag angle, zigzag length, Reynolds number, HTF temperature, and nanoparticle concentration, provide a comprehensive analysis of the critical factors influencing thermal performance. These parameters were selected based on prior literature and practical constraints to ensure relevance to real-world applications. The findings highlight fundamental heat transfer behaviours, such as the enhancement of convective heat transfer through vortex formation, the impact of geometric modifications on thermal performance, and the role of nanoparticles in improving phase transition kinetics. These insights are broadly applicable to other PCM-based thermal energy storage systems with similar heat exchanger structures.

The liquid fraction and average temperature profiles presented in Figs. 21 and 22 further corroborate the positive impact of nanoparticle addition on the solidification behavior of PCMs. The liquid fraction curves in Fig. 21 indicate that the presence of nanoparticles accelerates the solidification process, with higher nanoparticle concentrations leading to faster reductions in liquid fraction over time. The findings suggest that increasing the concentration of nanoparticles slightly accelerates the phase change process, leading to the complete melting of the PCM within 800 s. Conversely, in the case of pure PCM, only 95 % of the material melts after 3600 s due to some PCM's confinement at the top of the domain. This highlights the importance of incorporating nanoparticles in PCMs to improve their performance. The nanoparticles' high thermal conductivity and heat capacity play a crucial role in accelerating the phase change process. The average temperature of the PCM drops faster in the presence of nanoparticles than in the pure PCM. As shown in Fig. 22, the temperature drops dramatically at 50 s due to the high convection heat transfer caused by the significant temperature difference between the PCM and the HTF. The nano-PCM reaches thermal equilibrium at 15 °C, the same temperature as the HTF, while the pure PCM stabilises at 16 °C due to some liquid part remaining at the top of the domain. This observation underscores the advantage of using nanoparticles in PCMs, as they help to achieve thermal equilibrium more effectively.

This study also considers the analysis of the synergistic effects of incorporating both zigzag geometry and nanoparticle additives on the solidification performance of PCMs in a triplex-tube containment system. Fig. 23 quantitatively compares the solidification rate and time for four distinct cases: a straight channel configuration with pure PCM, a straight channel configuration with PCM incorporating 4 % Al_2O_3 nanoparticles, a zigzag channel configuration (67.5° angle and 15 mm length) with pure PCM, and a zigzag channel configuration with PCM incorporating 4 % Al_2O_3 nanoparticles. The data in Fig. 23 reveals that the zigzag geometry has a significantly

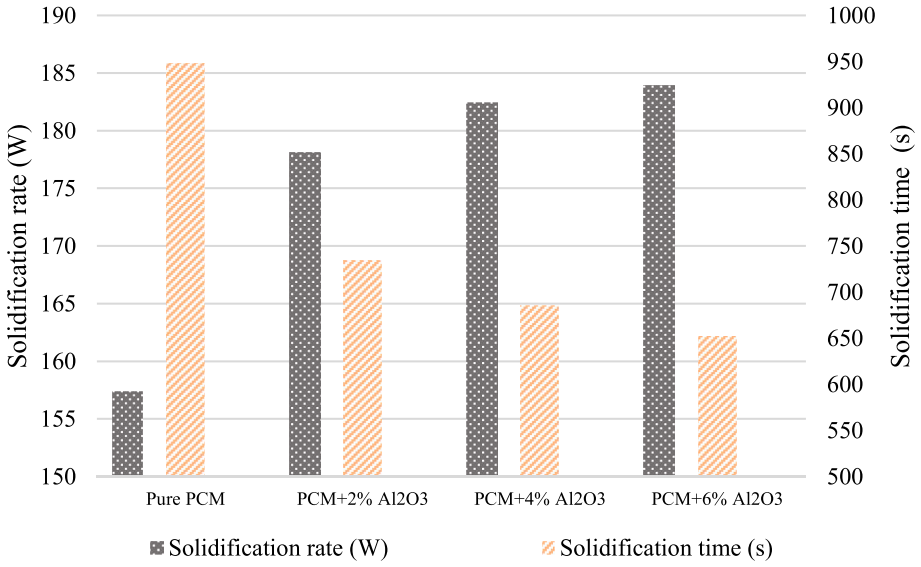

Fig. 20. The solidification rate and time for different concentrations of Al_2O_3 nanoparticles mixed with the PCM.

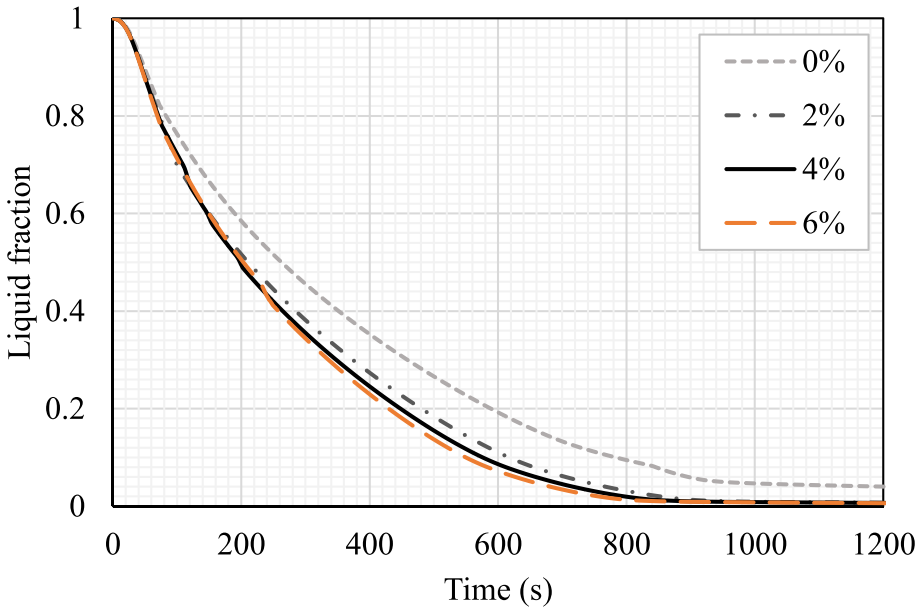

Fig. 21. Liquid fraction profile at different time steps using various concentrations of Al_2O_3 nanoparticles.

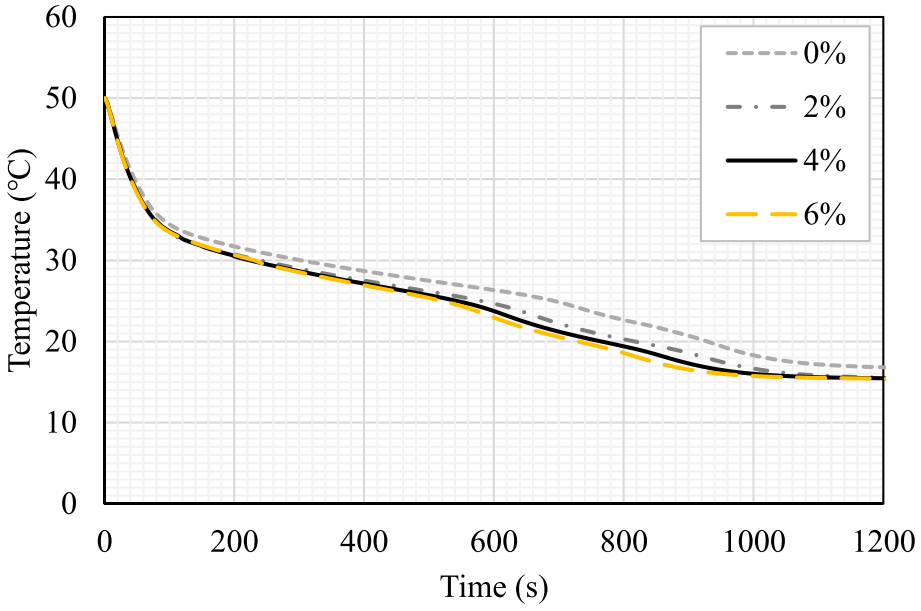

Fig. 22. The temperature profile at different time steps using various concentrations of Al_2O_3 nanoparticles.

more profound impact on enhancing the solidification performance compared to the nanoparticle addition. In the pure PCM cases, the zigzag channel configuration exhibits a remarkable 300 % higher solidification rate (157.4 W) and a 284 % shorter solidification time (948 s) compared to the straight channel configuration (39.6 W and 3645 s, respectively). This substantial improvement can be attributed to the increased heat transfer surface area and the promotion of vortex formation facilitated by the zigzag geometry, which collectively enhance the convective heat transfer and accelerate the solidification process.

While the zigzag geometry demonstrates a more significant impact, the addition of 4 % Al_2O_3 nanoparticles to the PCM also contributes positively to the solidification performance. In the straight channel configuration, the incorporation of 4 % Al_2O_3 nanoparticles leads to a 16 % increase in the solidification rate (from 39.6 W to 46.2 W) and a 14.7 % reduction in solidification time (from 3645 s to 3179 s) compared to the pure PCM case. Similarly, in the zigzag channel configuration, the addition of 4 % Al2O3 nanoparticles results in a further 16 % enhancement in the solidification rate (from 157.4 W to 182 W) and a 38 % decrease in solidification time (from 948 s to 685 s) relative to the zigzag case with pure PCM. These improvements can be attributed to the increased thermal

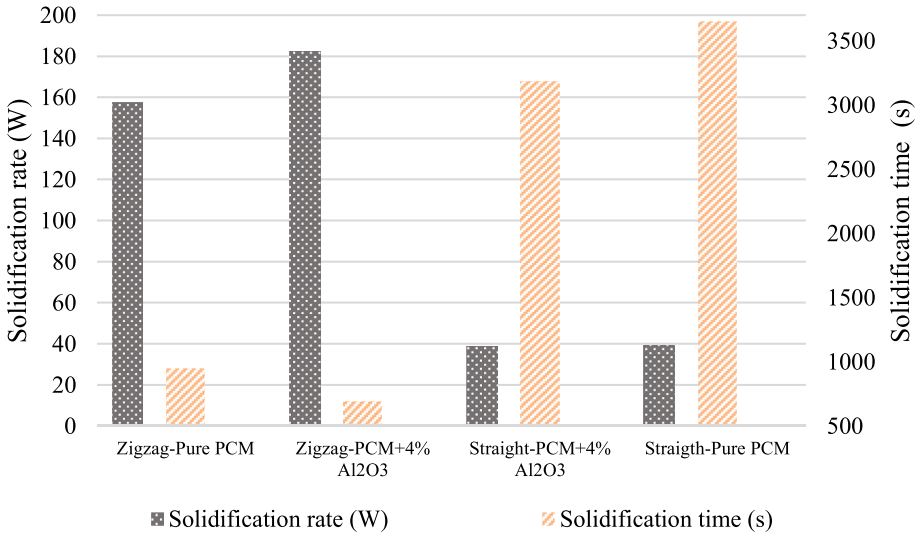

Fig. 23. The solidification rate and time for the straight and zigzag channel cases with and without Al_2O_3 nanoparticles.

conductivity and heat capacity provided by the Al_2O_3 nanoparticles, which facilitate more efficient heat transfer and accelerate the phase change kinetics within the PCM.

Fig. 24 presents the liquid fraction profiles for the same four cases analyzed in Fig. 23, providing a visual representation of the solidification progression over time. The data clearly illustrates the significant impact of the zigzag geometry on accelerating the solidification process. In the zigzag channel cases, both with and without nanoparticles, the liquid fraction decreases substantially faster compared to the straight channel cases, indicating a more rapid solidification rate. Specifically, in the zigzag case with pure PCM, 95 % of the PCM solidifies within 948 s, while in the straight channel case with pure PCM, only 5 % of the PCM solidifies within the same time frame. The addition of 4 % Al_2O_3 nanoparticles further accelerates the solidification process, with 95 % solidification achieved within 685 s in the zigzag case and 3179 s in the straight channel case.

Fig. 25 complements the analysis by depicting the average temperature profiles of the PCM for the four cases under investigation. The data shows a more rapid temperature drop in the zigzag channel cases compared to the straight channel cases, further corroborating the enhanced heat transfer facilitated by the zigzag geometry. Moreover, the presence of Al_2O_3 nanoparticles contributes to a faster temperature reduction in both the straight and zigzag channel configurations, indicating improved heat transfer and phase change kinetics. Notably, all cases reach an equilibrium temperature slightly higher than the inlet temperature of the heat transfer fluid

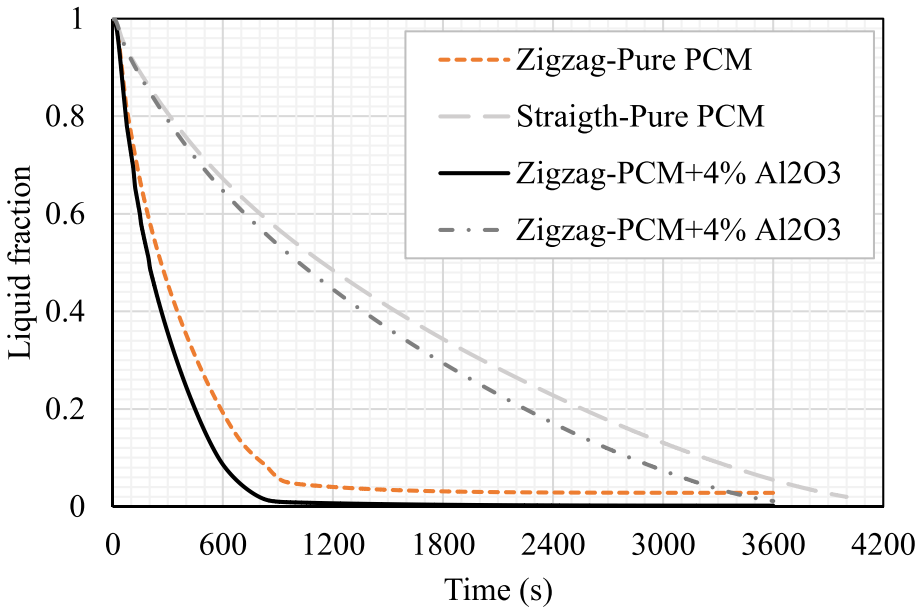

Fig. 24. The liquid fraction for the cases of straight and zigzag channels and with and without Al_2O_3 nanoparticles.

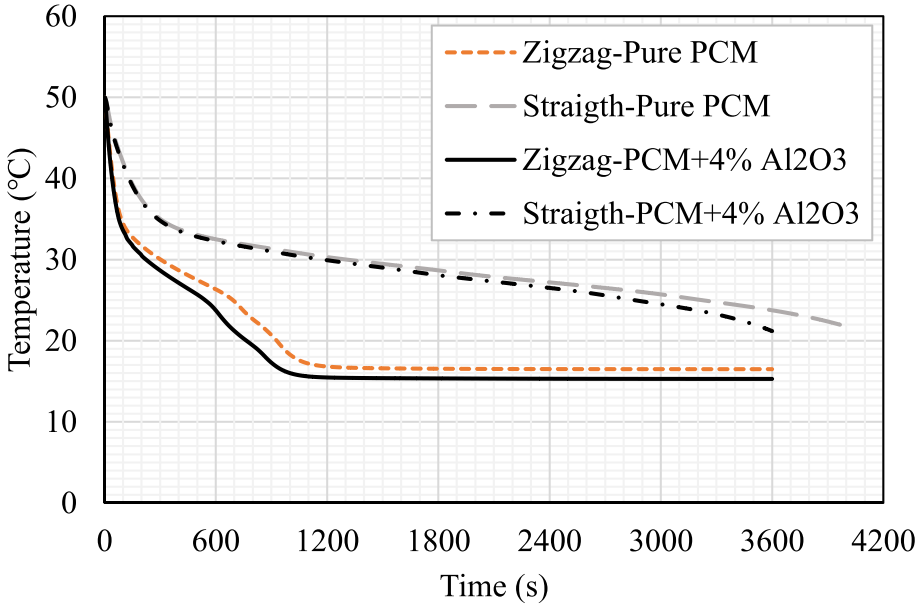

Fig. 25. The temperature for the straight and zigzag channels with and without Al_2O_3 nanoparticles.

(15 °C), which can be attributed to the presence of a small residual liquid fraction (approximately 5 %) at the top of the domain, acting as an insulating layer.

In summary, the zigzag geometry, particularly with a high zigzag angle of 67.5° and an extended length of 15 mm, exhibits a more profound impact on accelerating the solidification compared to the nanoparticle addition. However, the incorporation of 4 % Al_2O_3 nanoparticles provides further improvements in solidification rate and time, leveraging the increased thermal conductivity and heat capacity offered by the nanoparticles. The combination of these two approaches results in a remarkable 300 % enhancement in solidification rate and a 284 % reduction in solidification time compared to the baseline straight channel configuration with pure PCM. These findings are consistent with the trends reported in the literature. Mahdi et al. [30] reported that the incorporation of alumina nanoparticles at a 3–8 % volume fraction can enhance the solidification time by 8–20 % in a triplex-tube heat exchanger. The improvements observed in the present study, where the combination of a 67.5° zigzag angle and 4 % Al_2O_3 nanoparticles led to a 300 % increase in the solidification rate, align with and expand upon these previous findings. Furthermore, the influence of the zigzag geometry on the fluid flow patterns and the resulting enhancement in heat transfer is also consistent with the observations reported in the literature. Wang et al. [45] and Mahani et al. [46] studied the impact of zigzag configurations in plate-type heat exchangers and found that the zigzag geometry can significantly promote vortex formation and mixing, leading to improved melting and solidification rates of PCMs.

The findings showed a clear coupling relationship among the heat exchanger structural parameters, PCM properties, and overall thermal performance of the LHTES unit. The interactions between these various factors significantly influence the heat transfer rate, phase transition kinetics, and system efficiency. For example, increasing the zigzag angle of the heat exchanger tube enhances convective heat transfer by promoting vortex formation and fluid mixing. However, this geometric modification also affects the fluid flow resistance, which in turn impacts the overall pressure drop and pumping power requirements. Similarly, the addition of nanoparticles to the PCM improves the thermal conductivity, facilitating more efficient heat extraction, but it can also increase the viscosity of the PCM-nanoparticle suspension, affecting the fluid dynamics and heat transfer processes. The optimized parameters identified in this work, such as the 67.5° zigzag angle, 15 mm zigzag length, Reynolds number of 500, HTF inlet temperature of 10 °C, and 4 % Al_2O_3 nanoparticle loading, represent a balanced set of design choices that collectively maximize the solidification rate and minimize the solidification time. However, it is important to note that the identified optimal parameters may not necessarily represent the globally optimal solution, as there could be other combinations of design variables that can further improve the performance. Achieving true global optimization would require the adoption of more advanced techniques, such as multi-objective optimization methods (e.g., response surface methodology, genetic algorithms), which can simultaneously consider additional constraints and objectives, such as cost, long-term stability, and environmental impact.

While the current investigation focuses on the technical performance improvements of zigzag geometries, HTF flow conditions, and nanoparticle incorporation on the performance of LHTES systems, the assessment of the economic viability and practical implications of implementing these advanced designs is outside the scope of the present research. Future studies should explore the scalability of these improvements and incorporate techno-economic analyses to evaluate the operational costs, energy efficiency improvements, and potential cost savings. These considerations can better guide the development of cost-effective thermal energy storage solutions. Furthermore, the underlying heat transfer mechanisms reported in the current triplex-tube configuration suggest similar enhancements could apply to larger-scale systems and alternative geometries. These mechanisms include enhanced convective mixing,

increased heat transfer surface area, and improved phase transition kinetics. Future studies can explore the scalability of these enhancements by extending the analysis to larger heat exchanger designs. Additionally, integrating other geometric modifications, such as wavy or helical tube structures, could further optimize heat transfer performance.

6. Conclusion

This comprehensive study rigorously examined the effects of heat exchanger geometry, flow conditions, and nanoparticle integration on the solidification kinetics of PCMs within a zigzag-shaped triplex-tube latent heat storage system. The findings offer significant insights into the intricate interplay of conduction, convection, and phase change phenomena regulating thermal energy storage and release. The zigzag tube configuration emerged as a highly effective strategy to accelerate PCM solidification. Increasing the zigzag angle to 67.5° substantially augmented the heat transfer surface area and promoted vortex formation, enhancing convective heat extraction from the PCM. Further extending the zigzag length to 15 mm further expanded the contact area, leading to a remarkable 61.5 % reduction in solidification time compared to straight tube designs.

The flow conditions of the heat transfer fluid also played a crucial role. Elevating the Reynolds number from 250 to 500 enhanced forced convection, maintaining a greater temperature differential between the HTF and PCM and expediting the phase change process. Lowering the HTF inlet temperature from 20 °C to 10 °C created a more pronounced thermal gradient, accelerating solidification by 75 %. The incorporation of Al_2O_3 nanoparticles into the PCM provided an additional boost in performance. The high thermal conductivity of the nanoparticles facilitated more efficient heat transfer, diminishing localized temperature variations and promoting uniform solidification. The synergistic impacts of optimal zigzag geometry, flow augmentation, and 4 % Al2O3 nanoparticle dispersion resulted in a remarkable 300 % enhancement in solidification rate compared to the baseline straight tube configuration with pure PCM.

These findings highlight the complex interrelationship between structural design, fluid dynamics, and material properties in governing the phase change behavior of PCM-based thermal energy storage systems. The insights gained can guide the development of advanced latent heat storage solutions for diverse applications, including solar energy, waste heat recovery, and thermal management of electronics. Future research should explore the scalability of these improvements, investigate multi-objective optimization strategies, and examine supplementary enhancement techniques such as hybrid nanomaterials or active flow control mechanisms.

CRediT authorship contribution statement

Saleh Al Arni: Writing – original draft, Methodology, Formal analysis, Conceptualization. **Hakim S. Sultan Aljibori:** Writing – original draft, Investigation, Formal analysis. **Azher M. Abed:** Writing – original draft, Software. **Hayder I. Mohammed:** Writing – original draft, Validation, Software. **Jasim M. Mahdi:** Investigation, Formal analysis. **Hussein Togun:** Supervision, Project administration. **Abdellatif M. Sadeq:** Funding acquisition, Formal analysis. **Mohammad Ghalambaz:** Writing – review & editing, Visualization. **Nidhal Ben Khedher:** Writing – review & editing.

Declaration of competing interest

The authors declare that they have no known competing financial interests or personal relationships that could have appeared to influence the work reported in this paper.

Acknowledgement

The authors thank Qatar National Library for providing open access funding.

Data availability

No data was used for the research described in the article.

References

[1] A.M. Abed, H.R. Mouziraji, J. Bakhshi, A. Dulaimi, H.I. Mohammed, R.K. Ibrahem, et al., Numerical analysis of the energy-storage performance of a PCM-based triplex-tube containment system equipped with arc-shaped fins, Front. Chem. 10 (2022).
[2] F.L. Rashid, M. Eisapour, R.K. Ibrahem, P. Talebizadehsardari, K. Hosseinzadeh, M.H. Abbas, et al., Solidification enhancement of phase change materials using fins and nanoparticles in a triplex-tube thermal energy storage unit: recent advances and development, Int. Commun. Heat Mass Tran. 147 (2023) 106922.
[3] X. Sun, J.M. Mahdi, H.I. Mohammed, H.S. Majdi, W. Zixiong, P. Talebizadehsardari, Solidification enhancement in a triple-tube latent heat energy storage system using twisted fins, Energies (2021) 7179.
[4] H. Lund, Renewable energy strategies for sustainable development, energy 32 (2007) 912–919.
[5] M. Ebrahimnataj Tiji, H.I. Mohammed, R.K. Ibrahem, A. Dulaimi, J.M. Mahdi, Sh Majdi H, et al., Evaluation of T-Shaped fins with a novel layout for improved melting in a triple-tube heat storage system, Front. Energy Res. 10 (2022).
[6] A.H. Eisapour, M. Eisapour, H.I. Mohammed, A.H. Shafaghat, M. Ghalambaz, P. Talebizadehsardari, Optimum design of a double elliptical latent heat energy storage system during the melting process, J. Energy Storage 44 (2021) 103384.
[7] M.E. Tiji, J.M. Mahdi, H.I. Mohammed, H.S. Majdi, A. Ebrahimi, R.B. Mahani, et al., Natural convection effect on solidification enhancement in a multi-tube latent heat storage system: effect of tubes' arrangement, Energies 14 (2021) 7489.
[8] T. Watanabe, H. Kikuchi, A. Kanzawa, Enhancement of charging and discharging rates in a latent heat storage system by use of PCM with different melting temperatures, Heat Recovery Syst. CHP 13 (1993) 57–66.

[9] A. Sathishkumar, M. Cheralathan, Charging and discharging processes of low capacity nano-PCM based cool thermal energy storage system: an experimental study, Energy 263 (2023) 125700.
[10] M. Ferrara, F. Prunotto, A. Rolfo, E. Fabrizio, Energy demand and supply simultaneous optimization to design a nearly zero-energy house, Appl. Sci. 9 (2019) 2261.
[11] S. Bazri, I.A. Badruddin, M.S. Naghavi, M. Bahiraei, A review of numerical studies on solar collectors integrated with latent heat storage systems employing fins or nanoparticles, Renew. Energy 118 (2018) 761–778.
[12] J.M. Mahdi, E.C. Nsofor, Melting enhancement in triplex-tube latent thermal energy storage system using nanoparticles-fins combination, Int. J. Heat Mass Tran. 109 (2017) 417–427.
[13] F.T. Najim, S. Kaplan, H.I. Mohammed, A. Dulaimi, A.M. Abed, R.K. Ibrahem, et al., Evaluation of melting mechanism and natural convection effect in a triplex tube heat storage system with a novel fin arrangement, Sustainability (2022) 10982.
[14] Y. Wu, H.I. Mohammed, S. Chen, M. Luo, Y. Yu, Z. Zhou, Numerical investigation of the impact of toothed fins on the heat transfer performance of a shell-and-tube exchanger during phase change material melting process, Int. J. Heat Mass Tran. 217 (2023) 124637.
[15] X. Sun, H.I. Mohammed, M.E. Tiji, J.M. Mahdi, H.S. Majdi, Z. Wang, et al., Investigation of heat transfer enhancement in a triple TUBE latent heat storage system using circular fins with inline and staggered arrangements, Nanomaterials 11 (2021) 2647.
[16] H. Cui, J. Zou, Z. Gong, D. Zheng, X. Bao, X. Chen, Study on the thermal and mechanical properties of steel fibre reinforced PCM-HSB concrete for high performance in energy piles, Constr. Build. Mater. 350 (2022) 128822.
[17] H.S. Sultan, H.I. Mohammed, N. Biswas, H. Togun, R.K. Ibrahem, J.M. Mahdi, et al., Revolutionizing the latent heat storage: boosting discharge performance with innovative undulated phase change material containers in a vertical shell-and-tube system, Journal of Computational Design and Engineering 11 (2024) 122–145.
[18] M. Boujelbene, H.I. Mohammed, H.S. Sultan, M. Eisapour, Z. Chen, J.M. Mahdi, et al., A comparative study of twisted and straight fins in enhancing the melting and solidifying rates of PCM in horizontal double-tube heat exchangers, Int. Commun. Heat Mass Tran. 151 (2024) 107224.
[19] M. Boujelbene, H.I. Mohammed, H.S. Majdi, R. Babaei-Mahani, P. Talebizadehsardari, A. Rahbari, Melting performance of nano-enhanced phase change materials in a triple-tube heat exchanger with zigzag-shaped tubes, J. Energy Storage 67 (2023) 107484.
[20] A. Dinker, M. Agarwal, G. Agarwal, Heat storage materials, geometry and applications: a review, J. Energy Inst. 90 (2017) 1–11.
[21] A. Trp, K. Lenic, B. Frankovic, Analysis of the influence of operating conditions and geometric parameters on heat transfer in water-paraffin shell-and-tube latent thermal energy storage unit, Appl. Therm. Eng. 26 (2006) 1830–1839.
[22] P.T. Sardari, H.I. Mohammed, D. Giddings, G.S. walker, M. Gillott, D. Grant, Numerical study of a multiple-segment metal foam-PCM latent heat storage unit: effect of porosity, pore density and location of heat source, Energy 189 (2019) 116108.
[23] J. Tarragona, W. Beyne, A. de Gracia, L.F. Cabeza, M. De Paepe, Experimental analysis of a latent thermal energy storage system enhanced with metal foam, J. Energy Storage 41 (2021) 102860.
[24] J.M. Mahdi, E.C. Nsofor, Solidification enhancement in a triplex-tube latent heat energy storage system using nanoparticles-metal foam combination, Energy 126 (2017) 501–512.
[25] G. Asefi, T. Ma, R. Wang, Parametric investigation of photovoltaic-thermal systems integrated with porous phase change material, Appl. Therm. Eng. 201 (2022) 117727.
[26] J. Shen, H.I. Mohammed, S. Chen, B. Alkali, M. Luo, J. Yang, Mechanical vibration's effect on thermal management module of Li-ion battery module based on phase change material (PCM) in a high-temperature environment, Case Stud. Therm. Eng. 60 (2024) 104752.
[27] W. Zhou, H.I. Mohammed, S. Chen, M. Luo, Y. Wu, Effects of mechanical vibration on the heat transfer performance of shell-and-tube latent heat thermal storage units during charging process, Appl. Therm. Eng. 216 (2022) 119133.
[28] J.M. Mahdi, E.C. Nsofor, Solidification enhancement of PCM in a triplex-tube thermal energy storage system with nanoparticles and fins, Appl. Energy 211 (2018) 975–986.
[29] X. Sun, J.M. Mahdi, H.I. Mohammed, H.S. Majdi, W. Zixiong, P. Talebizadehsardari, Solidification enhancement in a triple-tube latent heat energy storage system using twisted fins, Energies 14 (2021) 7179.
[30] J.M. Mahdi, E.C. Nsofor, Solidification of a PCM with nanoparticles in triplex-tube thermal energy storage system, Appl. Therm. Eng. 108 (2016) 596–604.
[31] P.T. Sardari, H.I. Mohammed, D. Giddings, M. Gillott, D. Grant, Numerical study of a multiple-segment metal foam-PCM latent heat storage unit: effect of porosity, pore density and location of heat source, Energy 189 (2019) 116108.
[32] C. Nie, J. Liu, S. Deng, Effect of geometry modification on the thermal response of composite metal foam/phase change material for thermal energy storage, Int. J. Heat Mass Tran. 165 (2021) 120652.
[33] N.B. Khedher, J.M. Mahdi, H.S. Majdi, W.K. Al-Azzawi, S. Dhahbi, P. Talebizadehsardari, A hybrid solidification enhancement in a latent-heat storage system with nanoparticles, porous foam, and fin-aided foam strips, J. Energy Storage 56 (2022) 106070.
[34] A. Shahsavar, J. Khosravi, H.I. Mohammed, P. Talebizadehsardari, Performance evaluation of melting/solidification mechanism in a variable wave-length wavy channel double-tube latent heat storage system, J. Energy Storage 27 (2020) 101063.
[35] A. Shahsavar, A.A. Al-Rashed, S. Entezari, P.T. Sardari, Melting and solidification characteristics of a double-pipe latent heat storage system with sinusoidal wavy channels embedded in a porous medium, Energy 171 (2019) 751–769.
[36] O. Younis, A. Abderrahmane, M. Hatami, A. Mourad, G. Kamel, Thermal energy storage using nano phase change materials in corrugated plates heat exchangers with different geometries, J. Energy Storage 55 (2022) 105785.
[37] A. Mourad, A. Aissa, A.M. Abed, G.F. Smaisim, D. Toghraie, M.A. Fazilati, et al., The numerical analysis of the melting process in a modified shell-and-tube phase change material heat storage system, J. Energy Storage 55 (2022) 105827.
[38] A. Chibani, A. Dehane, S. Merouani, The sono-PCM reactors: a new approach for recovering the heat dissipated from ultrasonic reactors using a phase change material, Int. J. Heat Mass Tran. 215 (2023) 124505.
[39] A. Chibani, S. Merouani, H. Laidoudi, A. Dehane, C. Bougriou, Thermal management and electrical efficiency for concentrator photovoltaic systems using multiple phase change materials, Appl. Therm. Eng. 240 (2024) 122207.
[40] A. Chibani, A. Dehane, S. Merouani, O. Hamdaoui, Phase change material (PCM)-Based thermal storage system for managing the sonochemical reactor heat: thermodynamic analysis of the liquid height impact, Ultrason. Sonochem. 98 (2023) 106483.
[41] Y. Huang, Z. Deng, Y. Chen, C. Zhang, Performance investigation of a biomimetic latent heat thermal energy storage device for waste heat recovery in data centers, Appl. Energy 335 (2023) 120745.
[42] C. Zhang, Y. Huang, Y. Chen, Bionic study on latent heat thermal storage, Renew. Sustain. Energy Rev. 183 (2023) 113529.
[43] Y. Huang, D. Cao, D. Sun, X. Liu, Experimental and numerical studies on the heat transfer improvement of a latent heat storage unit using gradient tree-shaped fins, Int. J. Heat Mass Tran. 182 (2022) 121920.
[44] P. Talebizadehsardari, J.M. Mahdi, H.I. Mohammed, M. Moghimi, A.H. Eisapour, M. Ghalambaz, Consecutive charging and discharging of a PCM-Based plate heat exchanger with zigzag configuration, Appl. Therm. Eng. 193 (2021) 116970.
[45] P. Wang, D. Li, Y. Huang, X. Zheng, Y. Wang, Z. Peng, et al., Numerical study of solidification in a plate heat exchange device with a zigzag configuration containing multiple phase-change-materials, Energies 9 (2016) 394.
[46] R.B. Mahani, H.I. Mohammed, J.M. Mahdi, F. Alamshahi, M. Ghalambaz, P. Talebizadehsardari, et al., Phase change process in a zigzag plate latent heat storage system during melting and solidification, Molecules 25 (2020) 4643.
[47] Y. Ju, R. Babaei-Mahani, R.K. Ibrahem, S. Khakberdieva, Y.S. Karim, A.N. Abdalla, et al., Discharge enhancement in a triple-pipe heat exchanger filled with phase change material, Nanomaterials 12 (2022) 1605.
[48] A.A. Al-Abidi, S. Mat, K. Sopian, M. Sulaiman, A.T. Mohammad, Experimental study of melting and solidification of PCM in a triplex tube heat exchanger with fins, Energy Build. 68 (2014) 33–41.

[49] A.A. Al-Abidi, S. Mat, K. Sopian, M.Y. Sulaiman, A.T. Mohammad, Experimental study of melting and solidification of PCM in a triplex tube heat exchanger with fins, Energy Build. 68 (2014) 33–41.
[50] GmbH. Product information, data sheet of RT35 by rubitherm GmbH. https://www.rubitherm.eu/en/productcategory/organische-pcm-rt;.
[51] B. Águila, D.A. Vasco, P. Galvez, P.A. Zapata, Effect of temperature and CuO-nanoparticle concentration on the thermal conductivity and viscosity of an organic phase-change material, Int. J. Heat Mass Tran. 120 (2018) 1009–1019.
[52] Q. Wang, W. Wei, D. Li, H. Qi, F. Wang, M. Arıcı, Experimental investigation of thermal radiative properties of Al2O3-paraffin nanofluid, Sol. Energy 177 (2019) 420–426.
[53] Y. Ju, T. Zhu, R. Mashayekhi, H.I. Mohammed, A. Khan, P. Talebizadehsardari, et al., Evaluation of multiple semi-twisted tape inserts in a heat exchanger pipe using Al2O3 nanofluid, Nanomaterials (2021) 1570.
[54] C. Chen, H. Zhang, X. Gao, T. Xu, Y. Fang, Z. Zhang, Numerical and experimental investigation on latent thermal energy storage system with spiral coil tube and paraffin/expanded graphite composite PCM, Energy Convers. Manag. 126 (2016) 889–897.